Heritage Science

RESEARCH

Open Access

Corrosion prediction for preventive protection of aircraft heritage

Michal Kuchař[1*], Cyril Oswald[1], Jaromír Fišer[1], Miroslav Khol[2], Goran Simeunović[1], Tomáš Vyhlídal[1], Elodie Guilminot[3] and Jane Echinard[3]

Abstract

The paper presents a study on corrosion prediction for preventive aeronautical heritage protection, considering the aeronautical heritage stored or exhibited in an aviation museum. For the purpose of the study, the hangar with exhibited historical aircraft of significant cultural and societal value is located in the Aviation Museum Kbely, Prague, Czech Republic. Until now, such a preventive approach to protecting the aircraft heritage constituted from ancient aluminum alloys, in particular, has not been presented rigorously. Monitoring the hangar meteorological, pollution, and environmental data are acquired and interrelated with measured corrosion data to find a statistical model describing atmospheric corrosion in the hangar environment. The statistical model searched represents a Gaussian process based on a likelihood approach. As a result, the Gaussian process model is regressed to predict the corrosion of aluminum alloy-based artifacts in the monitored hangar with the marginal likelihood that is compared to machine learning-based prediction. Finally, it is shown that atmospheric corrosion is accurately predicted only when, among others, a synergistic effect of airborne pollutants and wind speed is considered.

Keywords Preventive approach, Aeronautical heritage, Aluminum alloy artifact, Pollution deposition, Gaussian process model, Likelihood approach, Machine learning

Introduction

From a historical perspective, metal corrosion had been observed as early as millennia B.C., but a significant increase in the corrosion has been observed since 1500s A.D. due to the advent of coal [1]. This trend due to sulfur dioxide exhalation continued until 1950 when the first regulatory actions on reducing pollutant exhalations emerged. In principle, the indoor heritage-built environment can be controlled somehow, but the outdoor conditions are beyond the human ability to change [2]. In this millennium, the effects of climate change have become the most critical issue to address. That is why heritage climatology has been introduced. Thus, the following parameter, the time of wetness (ToW), is considered to model and predict metal corrosion [3]. As an anticipated result of the ToW evolution calculated using environmental data from the Noah's Ark project, the ToW will increase in Northern Europe and reversely decrease in Southern Europe [4]. Nowadays, the preservation of cultural heritage must combine invasive and non-invasive methods to prevent corrosion through conservation interventions and the control of environmental factors that accelerate corrosion [5]. In the last decade, considerable attention has been paid to protecting industrial and cultural heritage [6]. This heritage covers historical buildings with unheated, non-air-conditioned indoor spaces for exhibiting technical objects, typically steam engines. Such historical buildings are also aircraft

*Correspondence:
Michal Kuchař
michal.kuchar@fs.cvut.cz
[1] Department of Instrumentation and Control Engineering, Faculty of Mechanical Engineering, Czech Technical University in Prague, Technická 4, Prague 160 00, Czech Republic
[2] Aviation Museum Kbely, Military History Institute Prague, Mladoboleslavská 425/9, Prague 197 00, Czech Republic
[3] Département de Loire Atlantique, GPLA-Arc'Antique, 26 rue de la haute forêt, Nantes 443 00, France

heritage buildings referred to as hangars, where historical aircraft are stored or exhibited. Regarding historical aircraft, the first flying structures constructed at the beginning of the 20th century through sandwich structures constructed before and mainly during the Second World War (WWII) [7], are primarily stored in aviation museums' hangars.

Historical aircraft to be safeguarded and kept for generations require invasive protection based on coatings. The invasive protection of heritage aircraft has already been provided in history through coatings as studied in [8]. The heritage aircraft and their parts (wings, fuselage) must be coated indispensably for outdoor protection rather than indoors. The protection becomes complex because the aeronautical heritage constitutes multi-material artifacts that are not only composed of aluminum alloys but also ferrous alloys, other metals, and non-metallic materials [7]. The prevailing alloy in heritage aircraft composition is duralumin, as reported in 1934 by [9]. To protect aluminum alloy materials in advance, the coating and the anodic layer need active corrosion protection [10]. In advanced protection, it is necessary to distinguish between wrought aluminum alloys [11], and cast aluminum alloys [12]. The cast aluminum alloys are somewhat more susceptible to localized corrosion. Moreover, the role of chemical composition in the corrosion of aluminum alloys is significant [13], particularly in outdoor conditions. Duralumin-type alloys suffer from delamination, intergranular, and pitting corrosion, as reported in [9] and later in [14]. This is opposed to pure aluminum that weakly corrodes because the spontaneously formed oxide layer is very protective [15]. Other metals, iron or steel, in contact with aluminum, contribute to galvanic corrosion, as exemplified in ancient [16], and modern aircraft [17]. Dissolution effects of galvanic corrosion of electrically coupled iron and aluminum alloys in seawater have been studied very recently [18]. Last but not least, a micro-galvanic coupling contributes to corrosion when this coupling is due to alloying elements used to strengthen the aluminum [19].

From the point of view of long-term atmospheric corrosion of aluminum, there is a bi-modal character of corrosion mass loss or pit depth versus the exposure time [20]. The objective is to enhance the long-term durability of aluminum alloys by preventing the formation of corrosive condensates. This is particularly important when the aluminum is exposed to polluted air, which consists of various gas mixtures [21]. Airborne pollutants, such as both sulfur dioxide and sulfides [22], chlorides [23], and both nitrogen oxides and ammonia [24], promote the corrosion of aluminum alloys, leading to pitting and crevice corrosion. These forms of corrosion lower the pollution threshold required for the continuation of corrosive processes [14]. Additionally, aluminum corrosion through exfoliation is common in coastal areas [25, 26]. Above a certain humidity threshold, corrosion increases substantially due to water sorption on the polluted surface. This threshold is attributed to 80% of air relative humidity but is highly inaccurate, as reviewed in [27]. It is observed that when the relative humidity of the indoor air remains below 60%, and the concentration of pollutants is minimal, thus preventing their deposition on the surface of artifacts, the corrosion rate is negligible in the short term [21]. While, for instance, the sulfur dioxide concentration is high enough to be deposited and the relative humidity is above 50%, the major aluminum alloys experience rapid corrosion in the form of hydrated aluminum sulfate [14]. In addition, the effect of higher temperature is corrosive for metals as concluded in [28] and demonstrated for aluminum in [29]. Furthermore, higher temperatures lead to the emission of acid vapors from wood-based pieces and other organic materials. These emissions accelerate the atmospheric corrosion of common metal elements [30–32]. Pollutants adsorbed on material surfaces persist long after the pollutants have been removed from the air [33]. Accounting for a difference between the surface conditions (relative humidity, temperature) and the ambient conditions (bulk air relative humidity, temperature), the moisture continues to absorb on polluted surfaces long after humid ambient air has been dried out [34]. Thus, the water sorption governed by surface pollutants occurs upon the surface relative humidity. Subsequently, the hygroscopic pollutants deposited on these surfaces dissolve into an electrolyte film under conditions of deliquescence relative humidity. This humidity level is typically lower than the surrounding indoor air [31, 35]. For contamination by chlorides, relative humidity as low as 35% can lead to iron corrosion, [36], where the chloride bringing about the corrosion already at such low relative humidity is magnesium chloride ($MgCl_2$). In the case of aluminum, the velocity of pollution deposition increases with both relative humidity of the air [37], and atmospheric particle size [38]. Furthermore, the deposition of pollution related to sulfur dioxide and chlorides is influenced by the shape of the exposed heritage material, whether it is deposited on wire or flat surfaces [39]. Sulfur dioxide infiltration into indoor spaces can exhibit a concentration less than half of that found outdoors [6]. In museum environments, passive Indoor Air Quality (IAQ) sensors are commonly used to monitor gaseous pollutants [40]. It is essential to distinguish between pollution level and dose thresholds when considering corrosion initiation [41]. Ensuring that corrosion is not present in typical museum environments over ten years is a more complex challenge than one year of no corrosion initiation. The pollution dose required

to initiate corrosion over ten years is significantly lower than that for a year. Additionally, the pollution threshold for corrosion initiation can be categorized based on electrochemical corrosion data, with distinct ranges for general and localized corrosion [42]. Notably, the threshold for localized corrosion is lower than for general corrosion, necessitating more stringent conditions to initiate corrosion in the same environment.

Besides the bi-modal character of long-term atmospheric corrosion of aluminum, there is also a bimodal character of particulate matter (PM) behavior outdoors and indoors [43]. Indoor air quality is affected by not equally distributed particles in the air concerning the particle size. Thus, there are the fine and coarse particle modes present in the air. Particles infiltrated from outdoors are mainly those belonging to an accumulation mode. The accumulation mode particles have lower deposition velocity as opposed to ultrafine (< 0.1 μm) and coarse (> 10 μm) particles that are captured with a higher deposition rate by and/or within historic building shell, for more details see [43, 44]. As a result, the fine particle mode prevails over the coarse particle mode indoors. On the other hand, different situations between the fine and coarse particle distributions in the air occur when high occupancy by visitors in the historic buildings takes place. Indoor particulate matter does not follow the trend of particulate matter outdoors. As presented in a heritage library study [45], the particle size with the highest indoor concentration results in 5 μm. This is due to the coarse particles brought in by an immense number of visitors transporting the dust from outdoors and indoors, as detailed on visitors' cloth dust transport in [46], tourism triggered resuspension in [47], visitor-carpet duo-effect in [48, 49], and finally inappropriate cleaning habits (dusting) in [50]. Consequently, the larger accumulations of bigger particles appear indoors, and the indoor-to-outdoor ratio in PM concentration increases with growing particle size so that this ratio results over one for naturally ventilated spaces, as a rule. Also, due to the library building's airtightness, the air exchange rate resulted in less than 0.5 h^{-1}, the common rate value for the naturally ventilated space, see [51]. Unlike the heritage library study in [45], the indoor-to-outdoor ratio in PM concentration meets values less than 1 even for the coarse particles, as presented in case studies on heritage archives and depositories in [43]. Obviously, these lower ratios are due to visitor-free operation regime of these archives and depositories when no or negligible accumulations of bigger particles are present. Notice that the air exchange rate resulted still lower than (0.3 h^{-1}) what was in the heritage library study in [45] because the archives and depositories are after reconstruction enhancing their airtightness. Given recent studies on the airtight heritage buildings the conveniently adopted indoor-to-outdoor ratio of $PM_{2.5}$ and PM_{10} concentration to be close to 1 in historical buildings without Heating, Ventilation, and Air Conditioning (HVAC) and any air filtering, see [41], needs to be updated. This ratio is to be updated due to nature of the case study (airtightness, occupancy, etc.) and the particle size. As well-known, coarse particles, i.e. dust, contribute to surface soiling indoors, see a soiling mechanism *per capita* in [52], and small particles, despite less mass carried, are deposited on surfaces in the form of fine, particularly combustion, particles, [44]. In addition, the fine particles are reactive with surfaces' material differently.

In relation to aluminum alloys, which predominantly comprise aeronautical artifacts, corrosion significantly contributes to aircraft degradation. The assessment of this corrosion typically involves exposure of metallic coupons as dosimeters at storage sites [53], and monitoring them by microscopy methods [54]. Metallic coupons and their analysis on corrosion in a laboratory provide the cumulative corrosion monitoring, and the shorter period of corrosion measurement analysis in the lab, the more expensive results this analysis for museums' stakeholders. Instead of applying metallic coupons, the corrosion can be evaluated directly by a microscopy method based on thermal aluminum deposition onto an optical fiber corrosion sensor, as detailed in [55]. This microscopy method advantage is its applicability to corrosion detection in aircraft structures. Next, the overall corrosiveness of the storage environment is evaluated based on standard ISO 9223, complemented by monitoring of corrosivity and air quality [23, 33, 56–59]. An advanced, non-destructive approach to corrosion monitoring involves measuring the oxygen consumption of cultural heritage artifacts [60]. On exhibition display, the oxygen consumption is measured inside Petri dishes (or watch glasses) that are glued to the surfaces of the large-scale artifacts (for instance, industrial or aeronautical heritage). An epoxy glue has been used for airtight adhesion of the small glass container, and an optical method based on luminescence is applied to oxygen concentration measurement inside the miniature glass container; for more details, see [61]. Indoor air quality is primarily based on the effectiveness of ventilation, filtration, and passive sorption [53]. The dosimeter method excels at detecting localized corrosion, whereas standardized approaches gauge the overall atmospheric corrosivity. Both methodologies are valuable for corrosion assessment in storage locations such as hangars. Given the stochastic nature of atmospheric corrosion and its discontinuous behavior, the applicability of chemical kinetic models to describe the corrosion process is somewhat limited [28]. Consequently, standardized statistical models are often preferred [62], and

extended statistical modeling, using environmental and corrosivity data, is increasingly used for corrosion prediction [63]. In particular, regression models exhibit limited efficacy in predicting aluminum corrosion ($R^2 < 0.6$) and are heavily influenced by geographical factors (terrestrial or coastal) [64–67]. As a result, non-parametric regression models are more suitable for aluminum alloys [63], with the Gaussian process (GP) model being robustly applied to specific interactive inputs for output prediction [68]. In fact, the Gaussian process model involves a kind of damage function using a latent function (alternatively interpreted with a kernel function) that is inferred by the Gaussian process in a non-parametric way. A crucial parameter in corrosion, linked to the temperature-humidity complex, is the Time of Wetness (ToW). The methodology for determining ToW is two-pronged: in outdoor conditions, it can be artificially simulated by wet and dry aging tests [69], or by moisture sensors [27, 70], while indoors, ToW is more an environmental than a surface parameter, considering factors such as dew and high humidity levels [4]. The application of ToW in evaluating atmospheric corrosivity in heritage aircraft hangars is discussed in [71].

A statistical approach to corrosion prediction becomes feasible when integrating various data types. This includes meteorological, pollution, and environmental data, as well as measurements of material corrosivity [63]. First, advancing the conventional regression methods, the statistical learning methods for corrosion process modeling have been introduced, as reviewed on their usage in [72]. Thus, a correlation analysis involving weight loss (or corrosion depth) of common metallic materials, including aluminum, has been conducted to start the corrosion modeling with parameters such as airborne pollutants and other environmental and meteorological parameters. The related statistical models obtained through regression analysis, particularly those that apply a cubic equation, have provided the best fit [73]. Pitting corrosion prediction for aluminum [74–76], and stainless steel [77], uses extreme value statistics based on pit depth probability distribution knowledge. The study in [78] replaces the extreme value distribution approach with the generalized lambda distribution method, offering a universal distribution family to model maximum pit depths. The evolution of aluminum's pit depth distributions over time has also been evaluated using the Monte Carlo method [79]. A Gaussian process regression is performed for modern aircraft corrosion prediction, which requires minimal prior knowledge of the corrosion model structure and parameters [63]. An alternative approach to modeling pit growth is corrosion image processing, which involves the extraction of the pixel histogram along with wavelet coefficients [80]. Automated corrosion detection from coupon corrosion image processing has recently been achieved through convolutional neural networks [81]. Popular techniques for atmospheric corrosion prediction include artificial neural networks [82], and support vector machines, the latter being capable of finding the global minimum [83]. In recent years, machine learning (ML) methods have emerged as powerful tools for corrosion prediction [84]. Kendall correlation analysis combined with gradient-boosting decision trees has been used to select input variables to predict corrosion rates using machine learning methods [85]. In this context, the *k*-nearest tree algorithm, random forest algorithm, support vector machine approach, and multilayer perceptron neural network are compared, with the random forest algorithm showing the best prediction accuracy. Indoor air quality prediction also benefits from developing machine learning models, where the XGBoost algorithm is preferred over the random forest algorithm [86].

The optimal strategy for preserving aeronautical heritage appears to blend invasive and preventive (i.e., non-invasive) protection methods. Focusing on preventive conservation, especially for materials like aluminum alloys commonly found in heritage aircraft, involves leveraging meteorological and pollution data for corrosion analysis [71, 87]. Only a handful of studies have historically addressed the protection and conservation of aluminum alloys in aeronautical heritage [9, 14, 88–90]. Furthermore, there is a notable absence of a systematic guide for safeguarding aluminum alloy-based aeronautical artifacts. However, recent initiatives include a project to investigate protective methods for aluminum materials in aeronautical heritage [91], and a comprehensive analysis of the preservation state of archaeological WWII aircraft [92].

In this paper, we develop and apply an enhanced statistical approach to corrosion prediction, mainly focusing on aluminum alloy components in aeronautical artifacts. Our methodology entails a likelihood-based approach for indoor corrosion prediction, requiring assessments of uncontrolled moisture inflow and pollution infiltration, [51], and the monitoring of environmental and corrosivity parameters. We adopt two methodologies—one from [63] and the other from [84, 85]—to suit the unique requirements of corrosion prediction in aeronautical heritage, with minimal prerequisite knowledge of the corrosion process. We demonstrate this approach through a case study on corrosion prediction-based preventive protection of aeronautical heritage, particularly within an aviation museum setting.

Methods

Heritage site description

The heritage site is the Aviation Museum Kbely [93], located in the capital, Prague, Czech Republic; see the site map in Fig. 1. This museum was founded in 1968 on the premises of the historic Prague-Kbely military airport, which was the first air base built after the creation of Czechoslovakia in 1918.

The abundance and quality of museum collections rank the Aviation Museum Kbely among the top European and worldwide aviation museums. Since 1968, its exhibitions have gradually grown from their original single hangar to the current five existing hangars covering nearly 5500 m^2 with permanent exhibitions together with another hall for occasional exhibitions and also an extensive open-air exhibition space, which altogether occupies an area of nearly 20,000 m^2 [94]. Currently, it has 275 aircraft in its collections, of which 129 aircraft, nearly 50 engines, and dozens of such aircraft parts as propellers, instruments, aviation equipment, and other items are displayed in individual hangars and unsheltered exhibition spaces. The other 136 aircraft are stored in depositories, and ten airworthy ones are in operation. Several airplanes belong to unique ones in the world. Namely, the first Czechoslovak military aircraft, Letov Š-2, and the first Czechoslovak commercial aircraft, Aero Ae-10, are exhibited/stored within aviation museums around the world only in the Aviation museum Kbely. Some aircraft can be owned privately (beyond museums) but in rare specimens. Regarding the indoor exhibitions, they are complemented by figurines in contemporary outfits representing flying and ground personnel, vehicles, and other equipment related to the security of air operations so that even a lay visitor can obtain some idea of the various historical periods involved.

The Aviation Museum Kbely is responsible for preserving and displaying a collection of aeronautical artifacts and items of historical, scientific, or artistic significance, offering them to the public through permanent and temporary exhibits. The fluctuating number of visitors compounds the challenge of maintaining stable climate conditions for aeronautical heritage preservation. The museum experiences peak attendance during the summer, while it remains closed to the public in winter. The operational season typically spans from May to October annually. Excluding the COVID-19 pandemic, the museum's visitor count during summer holidays or weekends averages about 800 per day, up to approximately 70,000 visitors annually. The capacity of each of the five exhibition hangars, designated for public tours, is limited to 30 visitors per tour. The museum manages around 25 tours daily in summer, divided almost evenly between morning and afternoon sessions. The impact of public attendance on the exhibited aeronautical heritage is most pronounced during the summer months, which also poses challenges due to heat waves, affecting not only the visitors and staff but also the artifacts. Last but not least, the adverse effect of visitors on the generation of

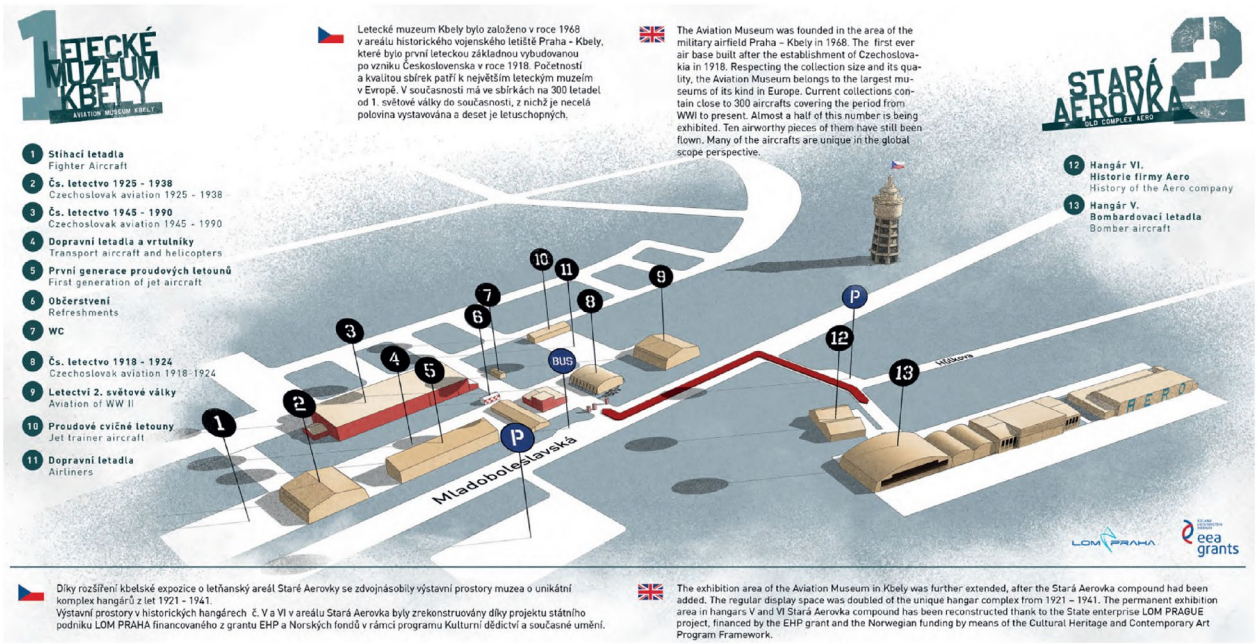

Fig. 1 Site map of the Aviation museum Kbely with six exhibition hangars marked with numbers 2, 3, 5, 8, 9, 10

coarse particles deposited on historical aircraft surfaces is ubiquitous.

In the following, the case study on corrosion prediction for preventive protection of aeronautical heritage is carried out considering the aeronautical heritage stored or exhibited in the Aviation Museum Kbely, Prague, Czech Republic.

Heritage site monitoring

First of all, the meteorological data for the Aviation Museum Kbely are acquired from Kbely Air Base—METAR LKKB (Meteorological Terminal Air Report). The Czech Hydrometeorological Institute brings in the airborne pollution overview based on the air quality index evaluated for the location of Prague-Kbely.

In a selected hangar of the Aviation Museum Kbely, the corrosivity of the atmosphere is monitored. The atmospheric corrosion logger, *AirCorr I* [95], has been installed indoors in the selected hangar of the Aviation museum Kbely, as shown in Fig. 2. The hangar selected is dedicated to General Karel Janousek; see the hangar with number 9 on the map in Figure 1, where the aeronautical heritage exhibited is linked to WWII. This heritage includes soviet fighter/ground-attack aircraft Ilyushin IL-2m3 Shturmovik and fighter Lavochkin La-7, next british trainer aircraft De Havilland DH-82A Tiger Moth Mk. II and Noorduyn Harvard Mk. IIB., and lastly, the French trainer aircraft Morane Saulnier MS-230. Another valuable aircraft exhibited is the German fighter aircraft Messerschmitt Me 262 Schwalbe; more details on aircraft heritage stored in the Aviation Museum Kbely are presented in [94]. The chosen aircraft for environmental and corrosivity data collection, Ilyushin IL-2m3 Shturmovik, as shown in Figure 2, is constituted of fuselage steel shell, duralumin wings and tail surfaces, wooden rear fuselage, and armored cockpit. Thereby the wooden rear fuselage is coated with fabric. Regarding De Havilland DH-82A Tiger Moth Mk. II it was also constructed with a wooden fuselage, while Morane Saulnier MS-230 is produced from plymax, a thin sheet of duralumin bonded to a thicker sheet of plywood. In the case of Messerschmitt Me 262 Schwalbe, its jet engine was made of mild sheet steel with an aluminum coating. A sandwich structure composed of aluminum alloy parts (beyond others) represents the historic WWII aircraft construction.

The logger *AirCorr I* measures the corrosion depth developed on the surface of sensing copper. Related environmental parameters, namely air temperature, relative humidity, and dew point, have been monitored by installing the *Eltek GDLM10* transmitter [96], in the place, see Fig. 3, adjacent to the placement of the logger *AirCorr I*. In Figure 3 anti-aircraft machine four-gun called Maxim 1910 is presented. In the hangar on WWII aeronautical heritage, the local microclimate (air relative humidity and temperature) is measured in 3 places distant 10 meters from each other and at a height of 1 meter above the ground. In only one of these places, the logger *AirCorr I* is located, see Fig. 2, to measure the corrosion depth of the sensing cooper. The measurement of corrosion in a single place is allowed because no different microclimates occur across all the places, characterizing the hangar environment. Proof on this fact, i.e., that the microclimates in the two other monitored locations in the hangar do not differ significantly from that at the logger *AirCorr I* location, is presented in Appendix A (A.1 Microclimates from three monitored locations).

Since aluminum alloys like duralumin undergo combined damage of pitting, intergranular, and exfoliation corrosions and thus lose their mass these alloys are suitable for the logger *AirCorr I* as sensor materials for long-term corrosivity monitoring, particularly when the sensor material, e.g. Al96Cu4, is exposed to aggressive

Fig. 2 Logger *AirCorr I* placement in the monitored hangar within aircraft Ilyushin IL-2m3 Shturmovik. Overall view (left). Detail on aircraft intake (right)

Fig. 3 Placement of transmitter GDLM10 from Eltek in the monitored hangar

environments (sea salt spray appearance), more details in [23]. On the other hand, this sensor material is unsuitable for low corrosive environments in sheltered exhibition sites of the Aviation Museum Kbely, see [71], to monitor the atmospheric corrosion. Instead, copper sensor usage is exemplified by monitoring metal corrosion in the aircraft (unheated) hangar of the Air and Space Museum at Le Bourget (France), see [57], despite this museum having one of the most important aircraft collections all over aviation history, from pioneers to nowadays. Details on the preservation state of the aluminum aeronautic collection in the Air and Space Museum at Le Bourget have been presented in [90]. In a low corrosive environment characterized by factors, namely higher air humidity and airborne (rather moderate) pollution constituted mainly by sulfur dioxide, nitrogen oxides, ozone, and Particulate Matter (PM), both the aluminum-copper alloy corrosion and the copper corrosion are sensitive to these factors, as detailed in [57, 97]. Thus, the sensor material used in the logger *AirCorr I* is copper concerning the corrosive effects caused by these factors, including (naturally ventilated) airflow in the monitored hangar.

The data acquired by the logger *AirCorr I* and the transmitter *GDLM10* are recorded in Fig. 4. In the subsequent Fig. 5, the detail of acquired environmental and corrosivity data is presented, showing these data during winter.

As apparent from the detail in Fig. 5, freezing-warming cycles around ±10°C take place, indicating potential water condensation/deposition; for more details, see Sect. Pollutant deposition determination.

Airborne pollution monitoring

Pollutants observed in the place of the monitored hangar are concerning inland and near-to-traffic locations as follows: SO_2, NO_2, O_3, $PM_{2.5}$, and PM_{10}. This air pollution characteristics is acquired by part from the weather station in Prague-Holesovice and the weather station in Prague-Riegrovy sady because the air pollution characteristics are not available in the weather station in Prague-Kbely at all. The nearest weather station from that in Prague-Kbely where both $PM_{2.5}$ and PM_{10} are measured is the weather station in Prague-Holesovice, located approx. 7 km from Prague-Kbely. Since both SO_2 and O_3 are not measured by the weather station in Prague-Holesovice, the nearest weather station to Prague-Kbely with such measurements is the weather station in Prague-Riegrovy sady. Note that the weather station in Prague-Riegrovy sady is situated in the location near to traffic as in case of the weather station in Prague-Kbely. The methods and principles of pollution data acquisition are presented in Table 1.

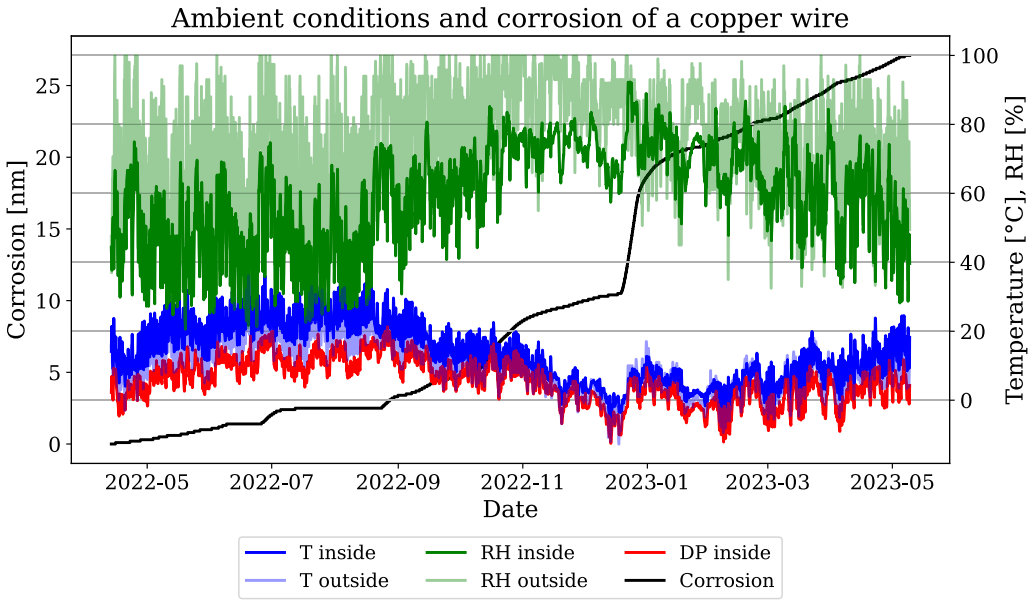

Fig. 4 Measured 1-year data

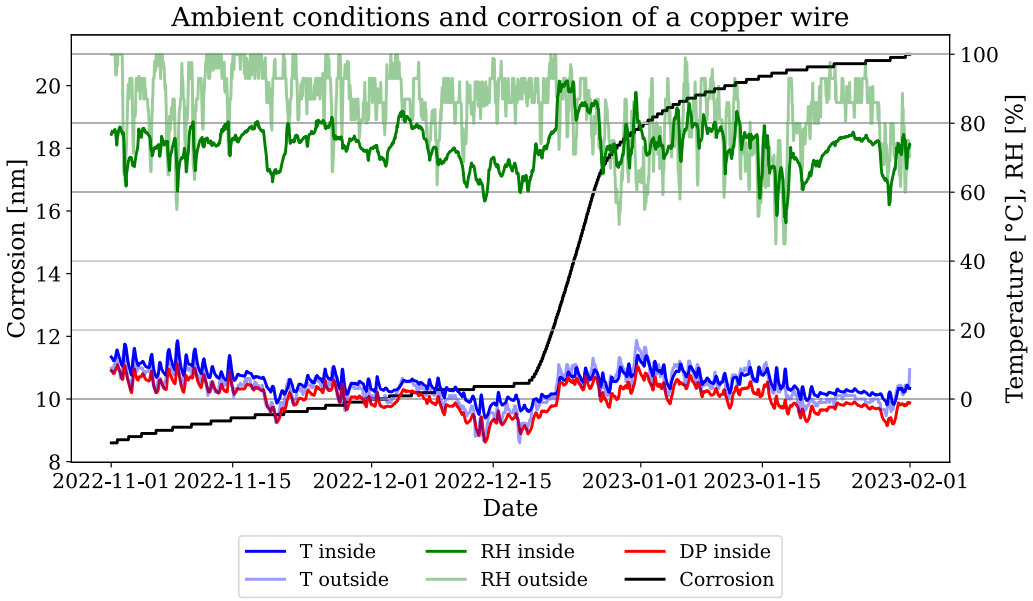

Fig. 5 Detail of Figure 4 within winter

Table 1 Pollution data aquisition

Pollutant	Measurement device	Method, principle	weather station
SO_2	TAPI[1], Model T100	UV-fluorescence	Prague-Riegrovy sady [98]
NO_2	TAPI[1], Model T200	Chemiluminescence	Prague-Holesovice [99]
O_3	TAPI[1], Model T400	UV-absorption	Prague-Riegrovy sady [98]
$PM_{2.5}$, PM_{10}	Environnement SA, MP101M Analyzer	Beta-ray absorption	Prague-Holesovice [99]

[1] Teledyne Advanced Pollution Instrumentation (TAPI)

Among other airborne pollutants, chlorides play a significant role because chlorides accelerate aluminum alloy corrosion. Generally, the chlorides constitute in part both $PM_{2.5}$ and PM_{10}, and the coarse fractions of PM_{10} are present in the air mainly during the winter due to traffic, residential heating, and also meteorological conditions. Thereby, the chlorides come mainly from the sea and deicing [100]. Despite sea salt spray having a negligible contribution to PM concentrations in the inland area of the Aviation Museum Kbely and there are no industries or incinerators in this area, the particulate chloride (NaCl) in the urban environment can constitute 7.4% of $PM_{2.5}$ and 11.2% of PM_{10} mass levels, for more details [101]. In the case of ammonium chloride, it constitutes up to 15% of the $PM_{2.5}$ mass as discovered in Utah, USA, during the winter in 2021 [102]. The effect of fine and coarse particles $PM_{2.5}$ and PM_{10}, respectively, on the aluminum alloy corrosion is investigated by correlation analysis in section Statistical modeling of aeronautical artifact corrosion. The measured outdoor concentration of gaseous pollutants, namely SO_2, NO_2, and O_3, and the particulate matter $PM_{2.5}$ and PM_{10}, within one year are recorded along with the thresholds for the minimal risk of aluminum alloy corrosion and pollutants' concentration calculated indoors in Fig. 7, presented in section Pollutant deposition determination. The wind speed which is significantly correlated with the atmospheric corrosion, for more details, see section Statistical modeling of aeronautical artifact corrosion, is recorded within one year in Fig. 6.

The measure of airborne pollution adsorption/absorption on the material surface is the surface removal rate given by

$$n_s = v_d \frac{A}{V}, \tag{1}$$

where A represents the exhibition area and V the hangar volume [103]. The corresponding pollution deposition velocity v_d can be measured or obtained from tabular data as reported in [37]. Then, considering the air exchange rate n in the monitored hangar and the surface removal rate n_s the averaged quasi-steady value of the infiltrated pollutant concentration is given [103]

$$C_i = \frac{n}{n + n_s} C_o. \tag{2}$$

In (2) C_o stands for the outdoor pollutant concentration. The thresholds for the minimal risk of aluminum alloy corrosion according to ASHRAE [104], are assigned with the following values, i.e. 2.62 $\mu g\,m^{-3}$, 4.88 $\mu g\,m^{-3}$, and 3.92 $\mu g\,m^{-3}$ for airborne pollutants SO_2, NO_2, and O_3, respectively, as shown in Fig. 7. In case of fine particles, $PM_{2.5}$, generated indoors this threshold is 1 $\mu g\,m^{-3}$, as also drawn in Fig. 7 in the next section. In case of particulate coarser than 10 μm, a threshold is to be established for cleaning up the heritage aircraft surfaces; for general rules, see [52]. This is more discussed in section Pollutant deposition determination. Based on the knowledge of pollutant deposition velocities on the material surface, the rates of pollutant deposition are calculated as follows:

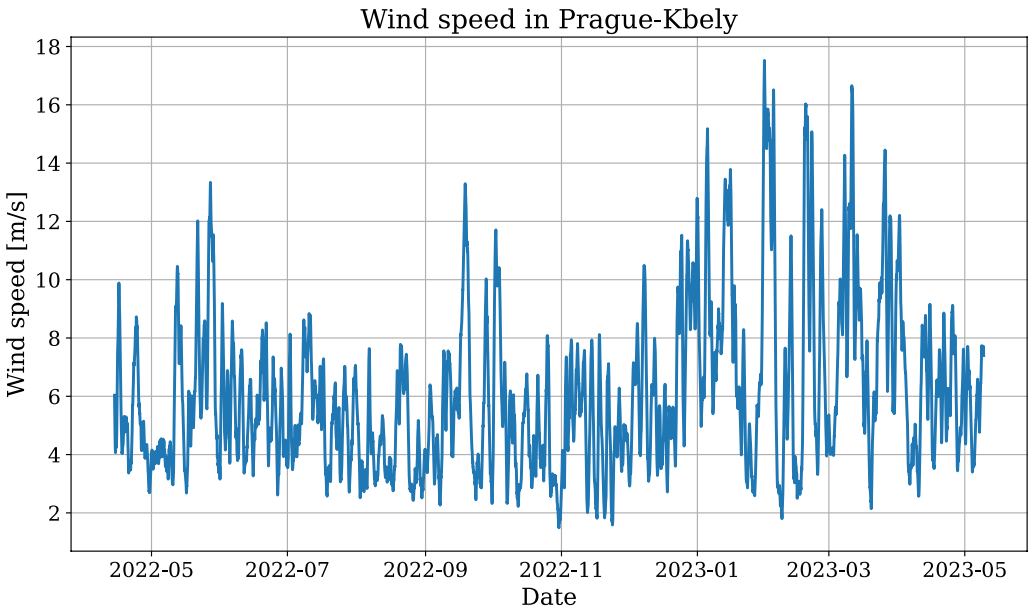

Fig. 6 One-year data of wind speed obtained from weather station in Prague-Kbely—daily averages

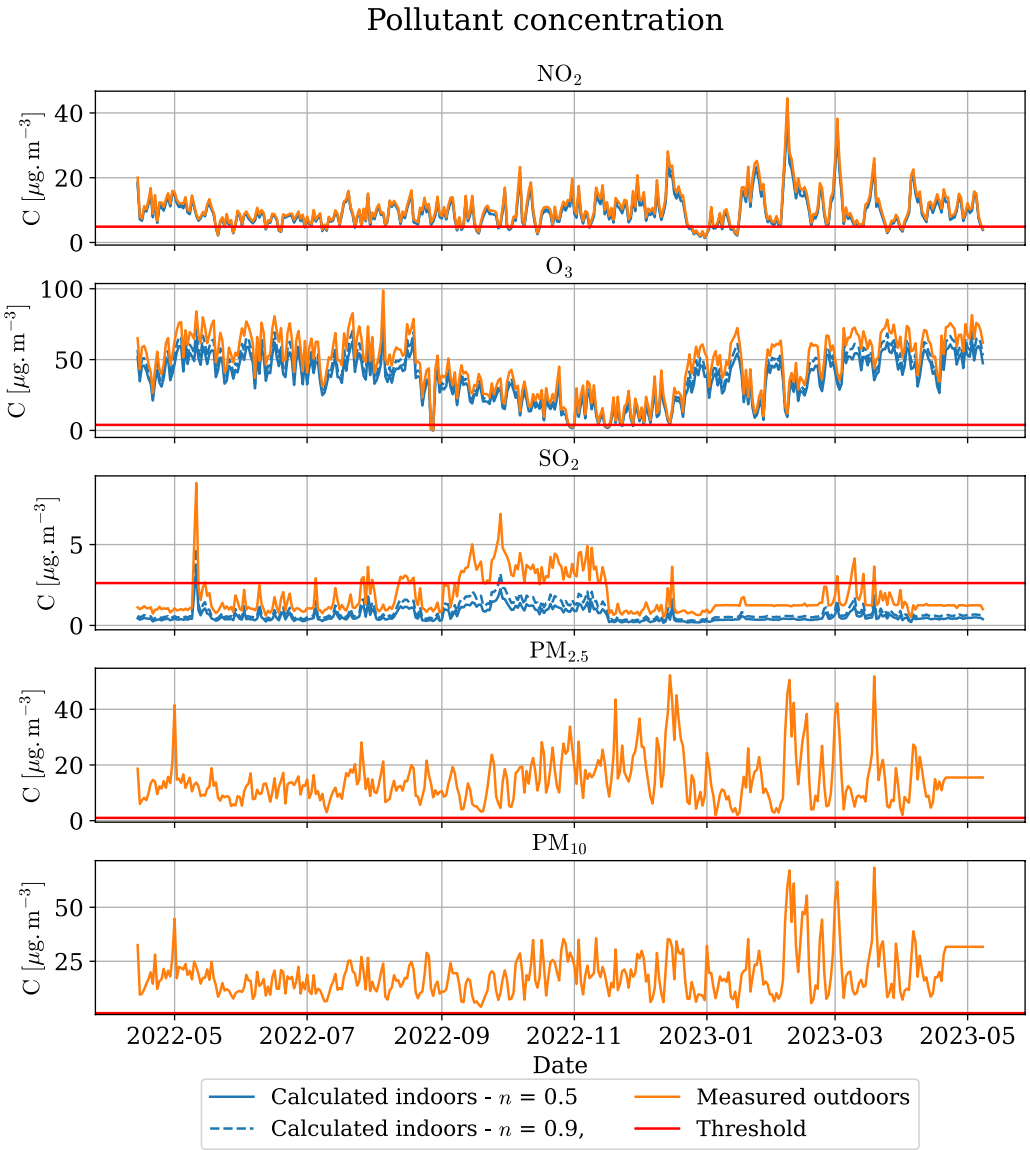

Fig. 7 One-year pollution data measured from weather stations in Prague-Holesovice and Prague-Riegrovy sady and indoor pollution calculated for min-max air exchange rate–daily averages

$$d = v_d \cdot C_i. \tag{3}$$

The following section determines the deposition of airborne pollutants present in the hangar environment on the aluminum material surface.

Results and discussion

Pollutant deposition determination

First, the pollutant infiltration is evaluated based on presumption of the air exchange rate in the monitored hangar environment and the surface removal rate. Because the air exchange rate has not been measured within the hangar operation this rate is ad hoc indicated 0.5 h^{-1}, the common value for naturally ventilated spaces. In the case of the airtight heritage buildings, as outlined in section Introduction, this rate can even drop below the common value, i.e., close to or below 0.3 h^{-1}. A sensitivity analysis concerning increasing this rate is provided when occupancy of the hangar by visitors is increased within the museum's season (May through October annually), in particular. Air exchange rate achieving 1 h^{-1} or a higher value brings in a moisture inflow and pollution infiltration into the hangar that can make the indoor climate seriously corrosive [51]. Indoor

spaces with air exchange rates over 1 h^{-1} are not naturally ventilated, and such spaces are with forced ventilation as a rule. Thus, the air exchange rate is mainly variable concerning museum operation (whether season or not). The museum's seasonal effect is suggested to be a major influence on the air exchange rate variability. Hence, the infiltration of airborne pollution accelerators of aluminum alloy corrosion, mainly SO_2, $PM_{2.5}$, and PM_{10}, is evaluated under varying (stepwise increasing) air exchange rate. For correlation analysis purposes in section Statistical modeling of aeronautical artifact corrosion, this rate is considered higher within the museum's season than in the off-season. While within the museum's season, three different rate values, i.e., 0.6 h^{-1}, 0.7 h^{-1}, and 0.9 h^{-1}, are considered, in the off-season this rate value could not be determined by a regression model analysis, for more details see section Comparison with machine learning models. On one hand, the increase in this rate from 0.5 h^{-1} through 0.9 h^{-1} brings a rather modest change in the infiltrated pollutant concentration; see Fig. 7. On the other hand, since the heritage aircraft hangars are not constructed with an airtight building shell, the air exchange rate, 0.5 h^{-1}, commonly expected as an upper bound for the airtight and naturally ventilated buildings, is overridden likely by a higher value. Consequently, even the most modest change effect (in case of SO_2) on pollutant deposition has to be considered as recorded in Fig. 8.

Regarding the surface removal rate n_s for aluminum, results with respect to environmental parameters in the hangar, particularly the relative humidity of indoor air as recorded in Fig. 4. This rate is recorded together with the deposition velocity v_d for SO_2, NO_2 and O_3 in Table 7, see Appendix B Pollution deposition on heritage aircraft surfaces.

To calculate the concentration of infiltrated airborne pollutants, the stepwise air exchange rates in the monitored hangar, i.e. $n = 0.5\ h^{-1}$, $n = 0.6\ h^{-1}$, $n = 0.7\ h^{-1}$, and $n = 0.9\ h^{-1}$, and the surface removal rates given by Table 7 are considered. Therefore, the averaged quasi-steady value of the infiltrated pollutant concentration is determined by (2). The concentrations of infiltrated SO_2, NO_2 and O_3 are then recorded in Fig. 7 together with the thresholds for minimal risk of aluminum alloy corrosion. Also, outdoor concentrations of ozone, sulfur dioxide, and nitrogen dioxide acquired from weather stations in Prague-Holesovice and Prague-Riegrovy sady are compared with the corresponding infiltrated pollutant concentration given by (2) in the following Fig. 7.

Despite the deposition velocities of gaseous pollutants SO_2, NO_2, and O_3 on aluminum in indoor spaces are variable with air relative humidity, in particular, this variability is well fitted with collected deposition data in Table 7. As regards $PM_{2.5}$ and PM_{10} they are experienced to be the indoor-to-outdoor ratio of their concentrations over 1 in naturally ventilated historical buildings, as summarized in section Introduction. This is because the coarse particulate, PM_{10}, fibers, and dust particles come from visitors' clothing, so the coarse particles are more generated

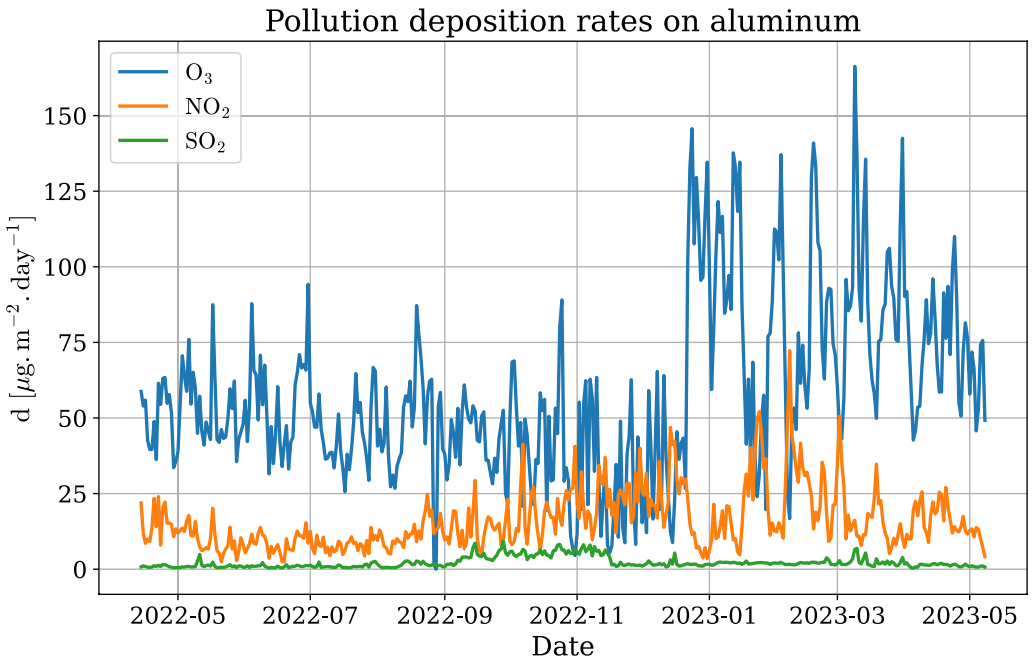

Fig. 8 Calculated pollutants' deposition rate on aluminum artifact surface when $n = 0.5\ h^{-1}$

indoors than infiltrated from outdoors. The next significant source of coarse particles in the monitored hangar is the carpets and turf rolls used for visitors to take a tour. Beneficially, the infiltration of PM_{10} into the monitored hangar is mitigated within the winter when outdoor coarse particles appear in particular because the museum is closed in the off-season (November through April on overturn of a year). The current precaution for mitigating coarse particulate deposits is based on cleaning up the heritage aircraft surfaces in the winter and before and after the museum's season. Particularly during the museum's season, the cleaning-up frequency must be increased to more than what is within the current precaution to decrease the aircraft surface cleaning threshold effectively. The increase in cleaning-up frequency limits the staffing problem the museum is experiencing.

Finally, the rates of pollutant deposition are calculated by (3) and recorded in Figure 8. Inspecting Fig. 8, it is clear that higher relative humidity inside the hangar corresponds to increased pollutant deposition rates. Particularly, throughout the measurement period, the deposition rates for NO_2 and O_3 are significantly higher than for SO_2. However, SO_2 poses a greater risk to corrosion of aluminum alloys, especially when the relative humidity (RH) exceeds 50%, as indicated by its higher surface removal rate, n_s (see Table 7). While the indoor infiltration of NO_2 and O_3 averages higher than that of SO_2, the deposition velocity of SO_2 is an order of magnitude greater compared to NO_2 and O_3.

The impact of SO_2 on aluminum alloy corrosion is such that the more SO_2 concentration exceeds its threshold, the lower is a relative humidity threshold for corrosion initiation due to formation of hygroscopic corrosion products. Unfortunately, the threshold of SO_2 concentration for corrosion initiation is the lowest of all the gaseous pollutants considered in this study, see section Airborne pollution monitoring. Despite this low threshold, as shown in Fig. 7, the indoor SO_2 concentration remains below this threshold for the corrosion initiation nearly everywhere within the period measured, hence the effect of SO_2 is less detrimental for the aircraft artifacts than it would be in case of this threshold overflow. Fortunately, there are no free air dewing events, as evidenced by the dew point data in Fig. 4. Moreover, deliquescence relative humidity is unlikely during the entire exposure period (over one year). However, the potential for moisture absorption on the polluted surface in the hangar cannot be disregarded. In certain conditions, especially when the hangar's ventilation is ineffective, the surface temperature of the material may drop below the dew point, leading to potential dewing on the aircraft's surfaces. Although the surface material temperature is not directly measured in the monitored hangar, dewing events on the aircraft materials are inferred, particularly at the location of the logger *AirCorr I*. This is suggested by the observed freezing-warming cycles during winter and spring, as shown in Figs. 4 and 5, where a notable increase in corrosion depth from 10 to 18 nm was recorded at the end of 2022. Particularly, the freezing-warming cycle between $-10°C$ and $+10°C$ is brought about by abrupt freezing at half of December 2022 and abrupt weather warming in a week, for more details, see Fig. 5. While aircraft surfaces persist cold after the warming, the surrounding air is warmed to $+10°C$. Other freezing-warming cycles appeared at the end of January 2023, within February 2023, and later in spring 2023 on a day-period basis between $\pm 3°C$ (or lower temperature range). The most detrimental for the aircraft heritage was the $\pm 10°C$ cycle, bringing about an abrupt increase in the corrosion rate (a slope of corrosion depth evolution in Fig. 5) after weather warming before Christmas in 2022.

Additionally, water deposition on the surfaces of historical aircraft is likely to occur in other areas of the hangar, not just near the logger *AirCorr I*, due to similar microclimates throughout the space, as proved and discussed in Appendix A (A.1 Microclimates from three monitored locations). Thus, the microclimates in the two other monitored locations in the hangar do not differ significantly from that at the logger *AirCorr I* location. Freezing and warming events, often not included into the time of wetness (an environmental parameter defined by [100]), do not account for the liquid state transitions of water vapor, such as condensation or hoar frost melting. However, recent evaluations of the hangar environment's corrosivity, as detailed in [71, 87], have employed the time of wetness. Despite this, a likelihood approach to atmospheric corrosion prediction is favored due to its rigorous modeling of the aircraft corrosion process.

Statistical modeling of aeronautical artifact corrosion

Correlation analysis

As pointed out in section Introduction, atmospheric corrosion is a stochastic process depending to some extent on variables monitored in the hangar, namely, air temperature and relative humidity, gaseous and particulate pollutants, in particular. Also the effect of air exchange rate that is variable with regard to hangar operation (whether within the museum season or not) should not be neglected. However, as explained in section Pollutant deposition determination, the air exchange rate is higher within the museum season. But, during the season period from May through October, the wind speed has decreased, see Fig. 6. This fact reflects the resulting correlation coefficient between the wind speed and the air exchange rate at -0.25, and this result does not show that the air exchange rate rises with increasing wind speed.

Then, an expectation that the air exchange rate grows with increasing wind speed is not proved. In addition, no correlation between the air exchange rate and the corrosion rate is found; for more details, see Appendix A (A.2 Lack of air exchange rate correlation). Due to this lack of correlation and the air exchange rate not being measured within the hangar operation, this rate is not included in the statistical modeling below. Instead, the wind speed is considered because, as proved in Appendix A (A.3 Null hypothesis of no wind speed effect) the wind speed is significantly correlated with the corrosion of aeronautical heritage. Regarding light irradiance, it has a marginal effect on metal corrosion. Hence, additionally, due to the hangar construction being built without windows, the effect of the light irradiance is not considered for corrosion evaluation. From the gaseous pollutants measured in the area of Aviation Museum Kbely, only sulfur dioxide turns out to be considered for analyzing the aluminum alloy corrosion, and also fine and coarse particles, i.e., $PM_{2.5}$ and PM_{10}, respectively. These particles include one type of their constituents, chlorides, present in the urban environment, that are also encountered in this area, see section Airborne pollution monitoring and discussion below. The correlation analysis of the stochastic process determines that from the known or measured quantities, the environmental parameters such as air humidity and temperature have the most significant impact on heritage aircraft corrosion. The levels of these correlations are recorded in the correlation matrix in Fig. 9. Figure 9 records the correlation among the following quantities summarized in Table 2.

The crucial inputs of the stochastic corrosion process, as evidenced by the correlation analysis, are the indoor air relative humidity, RH, and the indoor air temperature T. While the correlation analysis does not explicitly reveal the direct effect of gaseous pollution on aluminum alloy corrosion, the impact of sulfur dioxide and its deposition in the monitored hangar (as recorded in Figure 8) cannot be overlooked, as discussed in the forthcoming section (Gaussian process model). As regards the effect of $PM_{2.5}$ on aluminum alloy corrosion, it is not detected by the correlation analysis, either. Nevertheless, as explained in section Airborne pollution monitoring not only $PM_{2.5}$ but also PM_{10} contain chlorides that are present in the urban environment despite the apparent absence of sea salty aerosols. Hence, the chlorides as significant accelerators of aluminum alloy corrosion are also considered by involving fine and coarse particles in the corrosion process modeling below. Finally, the influence of wind speed, which does not show rather insignificant correlation (coefficient 0.24 in the correlation matrix in Fig. 9), contributes in reality to the corrosion process by acting as a carrier of gaseous pollution and moisture in the air. A synergistic effect of airborne pollution and wind speed on the corrosion takes place, as shown in section Comparison with machine learning models. To accept the wind speed as the next input into the GP model, the p-value of the null hypothesis that the wind speed does not affect the corrosion is determined at a value less than 0.001; for more details, see Appendix A (A.3 Null hypothesis of no wind speed effect). Strikingly, as a matter of severity from all the airborne pollutants measured, only the p-value in case of PM_{10} exceeds 0.001; thus, its value results in 0.48. Nevertheless, PM_{10} is involved in the statistical corrosion modeling due to chlorides participated on PM_{10}, as reviewed in section Airborne pollution monitoring. Note that the correlation analysis and statistical measures are evaluated for outdoor PM_{10} concentration. The concentration of coarse particles generated indoors is not measured or known. Still, their deposits on heritage aircraft surfaces are effectively mitigated as surveyed in section Pollutant deposition determination.

Table 2 Variables of stochastic corrosion process

Quantity	Symbol	Description
temp_in [°C]	T	Indoor air temperature
hum_in [%]	RH	Indoor air relative humidity
dew_in [°C]	T_{dew}	Dewpoint indoors
temp_out [°C]	T_{out}	Outdoor air temperature
hum_out [%]	RH_{out}	Outdoor air relative humidity
dew_out [°C]	$T_{dew_{out}}$	Dewpoint outdoors
SO_2 [$\mu g\, m^{-3}$]	C_{SO_2}	SO_2 concentration due to (2)
NO_2 [$\mu g\, m^{-3}$]	C_{NO_2}	NO_2 concentration due to (2)
O_3 [$\mu g\, m^{-3}$]	C_{O_3}	O_3 concentration due to (2)
$PM_{2.5}$ [$\mu g\, m^{-3}$]	$C_{PM_{2.5}}$	$PM_{2.5}$ concentration outdoors
PM_{10} [$\mu g\, m^{-3}$]	$C_{PM_{10}}$	PM_{10} concentration outdoors
windspeed [$m\, s^{-1}$]		Wind speed
winddir		Wind direction
qnh [hPa]		Pressure reduced to sea level
corrosion_diff [$nm\, h^{-1}$]	r	Corrosion rate

Gaussian process model

Based on the correlation analysis and statistical measures, the stochastic process of atmospheric corrosion is modeled as the Gaussian Process with four stochastic variables determined as follows: three input variables RH, T, and windspeed, and output variable r. Additionally, other inputs, given by pollutants present in the monitored hangar, namely C_{SO_2}, $C_{PM_{2.5}}$, and $C_{PM_{10}}$, are considered for modeling the GP. The two GP corrosion models (with and without pollutants considered) are compared to each other and simultaneously confronted

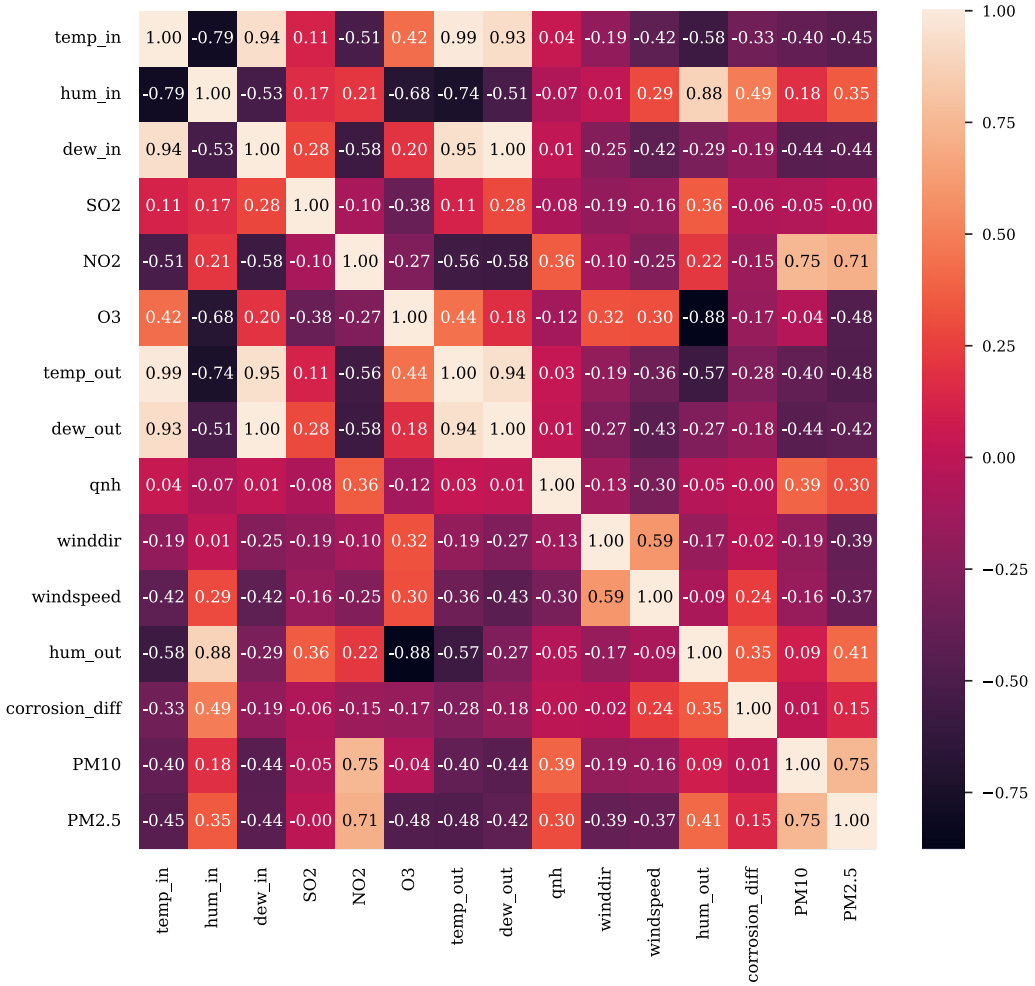

Fig. 9 Correlation matrix of measured variables

with measured one-year data of corrosion depth, see section Comparison with machine learning models.

Data preprocessing

The dataset covers 1 year and 25 days. The last 25 days are used for holdout prediction; see section Prediction of aluminum alloy artifact corrosion. The 1-year data were used for training and testing models. 80 % of the data were randomly shuffled and used for training. 20 % of the data were also shuffled and used for testing. Furthermore, the Moving Average (MA) filter was used. The window length was searched as a parameter within the training of the models. The best results are for the window of length 16 h. One more preprocessing step used in this research is Min-Max normalization, which performed better than standard normalization.

In case the last 50 days are used for holdout prediction, 80 % of the remaining data (after eliminating the last 25 days from 1-year data) were randomly shuffled and used for training. While 20 % of these remaining data were also shuffled and used for testing. Accuracy in prediction of aluminum alloy artifact corrosion is shown and compared with that accuracy in prediction in the case of both the last 25 days and the last 50 days of holdout predictions; for more details, see section Prediction of aluminum alloy artifact corrosion.

Comparison with machine learning models

The GP regressor was used and compared with other machine learning (ML) regressors using the PyCaret framework, which is an open-source ML library that simplifies the end-to-end model-building process [105]. PyCaret was chosen for its efficiency and ease of use, allowing rapid experimentation across multiple algorithms, and its emphasis on reproducibility, which aligns with the rigorous standards of scientific research. From frequently used ML algorithms and regressors (for more details, see section Introduction), the following regression methods are

Table 3 Comparison of regression methods[1]

Method	R^2	MAPE
Extra trees regressor	0.9147	0.2159
k-Neighbors regressor	0.8446	0.2597
Light Gradient boosting machine	0.8314	0.3645
Gaussian process regressor	0.7708	0.3068
Decision tree regressor	0.7478	0.2442
Gradient boosting regressor	0.7439	0.4802
AdaBoost regressor	0.6336	0.4220

[1] Regression under mean air exchange rate, $n = 0.5\ \mathrm{h}^{-1}$

Table 4 Comparison of 3 chosen regression methods

Method	R^2	MAPE
Extra Trees	0.9147	0.2159
k-Neighbors Regressor	0.8446	0.2597
Gaussian Process	0.7708	0.3068
Extra Trees[1]	0.8210	0.3136
k-Nearest Neighbors[1]	0.7601	0.3560
Gaussian Process[1]	0.6007	0.4988
Extra Trees[2]	0.6907	0.4379
k-Nearest Neighbors[2]	0.7027	0.4323
Gaussian Process[2]	0.5069	0.5453

[1] Regression not including SO_2, $PM_{2.5}$, and PM_{10} concentration as inputs

[2] Regression not including wind speed, SO_2, $PM_{2.5}$, and PM_{10} concentration as inputs

compared in Table 3 where MAPE stands for mean absolute percentage error. Other metrics, such as mean squared error (MSE), are not presented because there was no significant difference in these metrics between the regressors in Table 3.

From the comparison of the regressors in Table 3, the two most accurate models, namely *k*-Nearest Neighbors and Extra Trees, are selected along with the Gaussian Process model, which serves as a benchmark model to exceed in precision (R^2 close to 1 and MAPE close to 0). The results of these three models are presented in Table 4, and the parameters of the used models are detailed in Table 5. The results demonstrate a significant improvement when pollutants' concentration, C_{SO_2}, $C_{PM_{2.5}}$, and $C_{PM_{10}}$, are included as input variables. The most effective regressor emerges as the Extra Trees (ET) model with $R^2 = 0.915$ and MAPE = 0.215.

The regression analysis results, recorded in Tables 3 and 4, are obtained under the mean air exchange rate, $n = 0.5\ \mathrm{h}^{-1}$, for the naturally ventilated space. This is because the sweeping test, based on stepwise increasing n from $0.1\ \mathrm{h}^{-1}$ through $0.9\ \mathrm{h}^{-1}$, does not prove by means of R^2 value what is likely the air exchange rate. The reason why this rate cannot be determined stems from nearly linear dependence of relation (2) on n in limited (acceptable, $0.4\ \mathrm{h}^{-1} < n < 1\ \mathrm{h}^{-1}$) range of considered sweeping test.

The residuals of the trained models (GP, KNN, and ET) are analyzed and discussed in Appendix C Residuals of the trained models. For the ET regressor, there appears to be an overfitting effect on the training data. This phenomenon might be attributed to the nature of the measured corrosion data, which consistently increments in fixed steps. As seen in Fig. 5, the changes in measured corrosion values typically occur in increments of 0.1 nm. This increment corresponds to the resolution of the corrosion sensor used in the study. However, when trying to improve the Extra Trees (ET) model by reducing its number of trees, its ability to predict accurately decreased.

Prediction of aluminum alloy artifact corrosion

The prediction was evaluated on 25 days of measurement, which was not included in training and testing. The comparison of all three chosen models in the whole (not shuffled) dataset is shown in Fig. 10. The detailed prediction is shown in Fig. 11. The prediction evaluated on 50 days of measurement are added for comparison into both Figs. 10 and 11.

The study modeled a copper wire's corrosion, miming aluminum alloy corrosion in sulfur-rich air with fine and coarse particles. This modeling used shuffled data from one year. The results showed that the Extra Trees (ET) regressor had an R^2 value of 0.915, the *k*-Nearest Neighbors (KNN) regressor had 0.845, and the Gaussian Process (GP) regressor had 0.771. These findings are detailed in Table 4 for the mean air exchange rate. In the first two weeks of prediction, the two best models: ET and KNN-predicted corrosion, closely aligned with the actual data while the GP model underestimated the corrosion with an error close to 0.5 nm, as shown in Fig. 11. However, after two weeks of prediction, reversely, the GP model tended to overestimate the corrosion, with an error substantially exceeding 1 nm. Despite the GP regressor being less accurate in predicting

Table 5 Parameters of used models

GP kernel	GP likelihood function	GP optimizer	ET number of trees	ET criterion	KNN neighbors	KNN metric
RBF	Log-marginal-likelihood	L-BFGS-B	100	Squared error	5	Minkowski

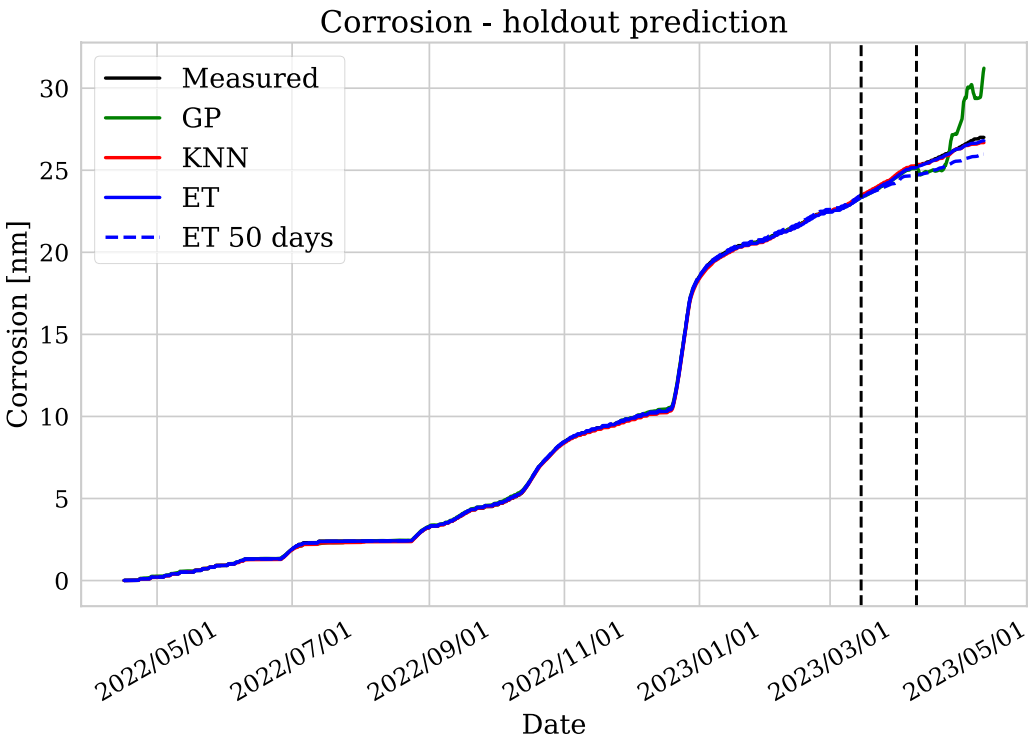

Fig. 10 Comparison of the three chosen regression methods: Gaussian Process (GP), *k*-Nearest Neighbor (KNN), and Extra Trees (ET) for the whole length of measurement

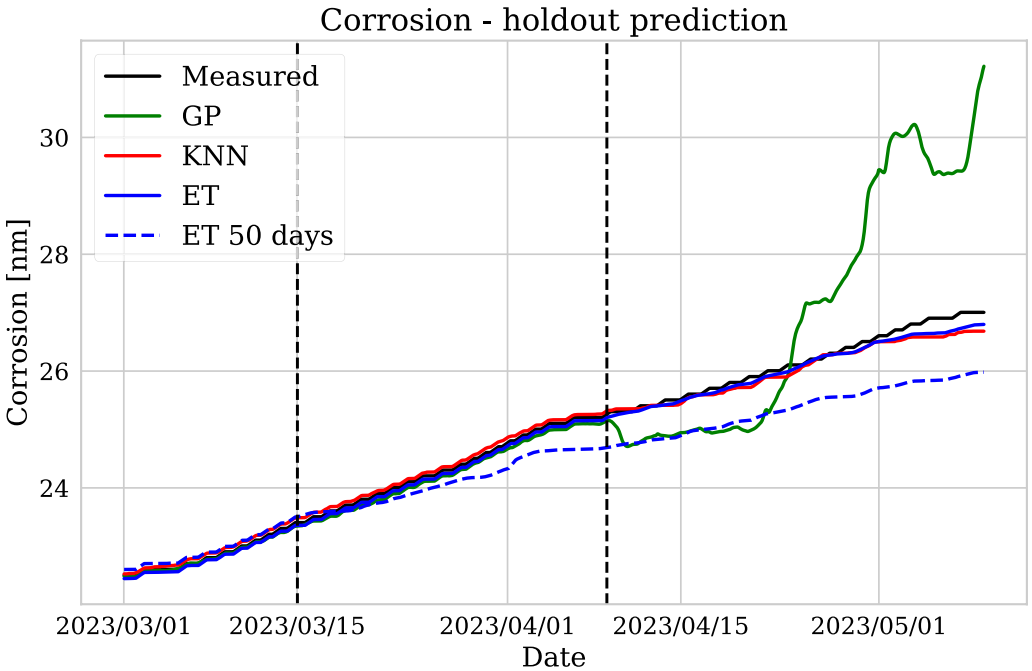

Fig. 11 Hold out prediction for both the last 25 days and the last 50 days. Comparison of all three chosen regression methods: Gaussian Process (GP), *k*-Nearest Neighbor (KNN), and Extra Trees (ET). The case with 50 days prediction demonstrated on the best regression method, ET

the corrosion, as shown in Table 3, it serves as a basic standard. Other machine learning methods should aim to exceed this standard, particularly in accuracy. For further discussion, it is necessary to collect at least another year of data.

Eliminating the wind speed and airborne pollutants, namely sulfur dioxide, fine and coarse particles in particular, from inputs of the stochastic process, the R^2 is by 0.2 worse for the chosen models. On the other hand, with the improvement of indoor air quality, the duralumin corrosion rate would be decreased, particularly when no synergistic effect of airborne pollutants and wind speed is in play.

The statistical approach presented in this study is unique in its rigorous elaboration of aircraft corrosion prediction for preventive protection of the aeronautical heritage. Only the statistical approach from [63] is similar in the application of the Gaussian process, where, however, corrosion of modern aircraft has been predicted, and the surface conductivity of the aircraft is required to measure or estimate.

From corrosion evaluation/prediction indoors, the effect of material surface quality on atmospheric corrosion is indicative in water and pollutant deposition, nevertheless significant for preventive conservation of aeronautical heritage. While, in outdoor conditions, the composition of aeronautical heritage material has a considerable effect on corrosion and its type, as recently investigated in [91].

Future perspectives and challenges

The corrosion model is expected to track corrosion over longer periods, such as 50 days or more. However, this will require comprehensive and extensive historical data sets. These data sets should include details on corrosion progression, humidity and temperature fluctuations, pollution levels, moisture inflow, and other weather parameters (especially wind speed). Last but not least the air exchange rate variability falls into the data sets needed for the corrosion prediction. However, one is to be aware that there is a difference in the air exchange rate between the naturally ventilated spaces and the spaces with forced ventilation. While in the case of the naturally ventilated hangar, the air exchange rate effect on the corrosion of aeronautical heritage has not been discovered (also due to missing rate data measurement) in the case of the aircraft building with the forced ventilation (but without pollution filtration and heating) this rate effect on the corrosion exists very likely.

As opposed to the air exchange rate effect (in a naturally ventilated hangar), the wind speed effect on atmospheric corrosion within the hangar is very likely, as proved in the case of the Aviation Museum Kbely. In fact, airborne pollution and wind speed have a synergistic effect on atmospheric corrosion that the speed of the wind contributes to the corrosion process by acting as a carrier of airborne pollutants and moisture in the air. What rests on uncovering the potential correlation between the air exchange rate and the wind speed in the case of the hangar with forced ventilation.

The machine learning (ML) approach to predict atmospheric corrosion in heritage aircraft shows promising transferability to terrestrial regions with moderate climates. However, for coastal areas, it is necessary to incorporate additional inputs, particularly the effects of chlorides (sea salt spray), into the Gaussian Process (GP) or ML models. Despite this, the structure of the GP or ML models should remain capable of accurate atmospheric corrosion prediction. For model validation, it is essential to use sensing materials such as aluminum alloys or other metals that are more stable yet sensitive to chlorides. A notable challenge lies in adapting this ML approach to predict heritage aircraft corrosion in tropical or cold climates. It is desirable to fine-tune selected ML models in the future.

From the case study focused on the protection of the aeronautical heritage, it becomes clear that the monitored hangar requires heating to prevent freezing-warming cycles. This heating must consider an air exchange rate optimized for corrosion prevention, which should be adapted to outdoor conditions to minimize the moisture inflow and the pollution infiltration. An ideal air exchange rate is achieved when a balance is struck between the infiltration of outdoor conditions (including pollution and moisture content) and the indoor influences such as moisturizing, VOC content, and dust generation that impact aircraft corrosion. In the monitored hangar, despite the presence of a high-power HVAC system, it remains unused due to the high cost of operation.

To mitigate water condensation/deposition on the aircraft surface, intermittent heating of the hangar is suggested in critical spaces for corrosion. Therefore, low-power heating and ventilation units should be installed only for localized microclimate control. Then, the aeronautical heritage will remain protected, and simultaneously, the energy operation cost will be decreased opposite to the central (high-power) HVAC unit. Another mitigation precaution is to retrofit or reconstruct the monitored hangar to improve the isolation of the hangar construction or the ventilation of airflow through the installation of barriers. Next, the wooden pavement will be installed instead of the carpets and turf rolls used for visitors to take a tour in the monitored hangar. The heritage aircraft are also to be treated (finishing, paints) to increase aluminum alloy

surface quality to decrease water and pollution deposition. Regarding the museum's collection exhibited outdoors, invasive methods of aircraft protection will be considered in the future, applying or restoring a coating on historical aircraft surfaces.

Conclusions

This research investigates the corrosion of aeronautical heritage artifacts stored in hangars through the Gaussian process and machine learning modeling. This study focuses specifically on the corrosion of materials based on aluminum alloy, which is exacerbated by the harmful environmental conditions within these hangars. A case study is conducted using more than one year of environmental and corrosion data collected from a heritage aircraft hangar. This study examines the effectiveness of three different regression and machine learning methods—Gaussian Process regressors, *k*-Nearest Neighbors, and Extra Trees—in predicting the corrosion depth on aircraft surfaces. The findings reveal that *k*-Nearest Neighbors and Extra Trees methods outperform other regression methods, using Gaussian Process regression as a benchmark for accuracy.

The corrosion depth development is monitored using a copper sensor, particularly in poorly ventilated areas of the hangar. This sensor indicates localized corrosion, which, due to similar microclimates in other two monitored areas of the hangar, suggests that similar corrosion is likely to occur in these locations as well. A significant limitation of the case study is its reliance on data solely from the Aviation Museum Kbely, with no comparative data from other heritage sites with historical aircraft. For more robust model training and longer corrosion prediction, collecting data spanning at least two years is necessary.

Appendix A: Correlation analysis and statistical measures

A.1 Microclimates from three monitored locations

As claimed in section Heritage site monitoring, the measurement of corrosion in a single place (see location of the logger *AirCorr I* in Fig. 2) is allowed because no different microclimates occur across all the places, characterizing the hangar environment. This fact, i.e., that the microclimates in the other two monitored locations in the hangar do not differ significantly from that at the logger *AirCorr I* location, is proved by correlation analysis among ambient variables measured in three locations of the hangar. Resulting correlation matrix among these variables is presented in the following Table 6.

The Table 6 shows that air temperatures and relative humidities from three locations within the monitored hangar are correlated to each other. Hence, the measurement in only one place is justified to be used for the corrosion model training and model-based corrosion prediction.

A.2 Lack of air exchange rate correlation

The air exchange rate is variable with respect to hangar operation (whether within the museum season or not), in particular, for more details, see section Pollutant deposition determination. Expecting the air exchange rate growth with increasing the wind speed, there exists a correlation between the air exchange rate and the wind speed. Performing the correlation analysis, the correlation coefficient between the air exchange rate and the wind speed results in −0.25. However, this result contradicts the expectation, and reversely, during the museum season period from May through October of a year when the air exchange rate is increased, the wind speed is decreased (see Fig. 6). This fact is not approved with the correlation coefficient resulting in insignificant −0.25, nonetheless the expectation that the air exchange rate increases with the wind speed is not proved. In addition,

Table 6 Correlation matrix among ambient variables from three locations

	RH	$^{a}RH_1$	$^{b}RH_2$	T	$^{a}T_1$	$^{b}T_2$
RH	1	1	1	−0.79	-0.78	−0.79
$^{a}RH_1$	1	1	1	−0.78	−0.77	−0.77
$^{b}RH_2$	1	1	1	−0.78	−0.77	−0.78
T	−0.79	−0.78	−0.78	1	1	1
$^{a}T_1$	−0.78	−0.77	−0.77	1	1	1
$^{b}T_2$	−0.79	−0.77	−0.78	1	1	1

[a] T_1 and RH_1—air temperature and relative humidity in the first of other two locations.

[b] T_2 and RH_2—air temperature and relative humidity in the second of other two locations.

Table 7 Surface removal rates on aluminum

RH [%]	0	25	50	75	90
SO_2					
v_d [cm s^{-1}] [a]	0	0.001	0.002	0.007	0.01
n_s [h^{-1}][d]	0	0.013	0.026	0.092	0.131
NO_2					
v_d [cm s^{-1}][b]	0	0.0005	0.0015	0.0027	0.0034
n_s [h^{-1}][d]	0	0.007	0.02	0.035	0.045
O_3					
v_d [cm s^{-1}][c]	0.00063	0.00068	0.0014	0.0032	0.0054
n_s [h^{-1}][d]	0.008	0.009	0.018	0.041	0.071

[a] SO_2 deposition velocities on aluminum.

[b] NO_2 deposition velocities on aluminum.

[c] O_3 deposition velocities on aluminum.

[d] Surface removal rates given by (1) where $A = 2976$ m^2 and $V = 7884.8$ m^3

no correlation between the air exchange rate and the corrosion rate is found; thus, the correlation coefficient results close to zero.

A.3 Null hypothesis of no wind speed effect

To accept the wind speed as the next input into the GP and machine learning models, the p-value of the null hypothesis that the wind speed has no effect on the corrosion is determined at value less than 0.001, using the t-test. Hence the wind speed and its synergistic effect on the atmospheric corrosion of the aeronautical heritage becomes very likely.

Appendix B: Pollution deposition on heritage aircraft surfaces

The surface removal rate values for aluminum are evaluated from deposition velocities as specified in Table 7 (for more data, see footnote 4) below. Thereby the deposition velocity values are obtained from tabular data reported in [37], which are linearly interpolated (and extrapolated up to 100% relative humidity) for data acquired over one year from the Aviation Museum Kbely, Prague, Czech Republic (see Fig. 4).

Note that the effect of air exchange rate variability on the pollutant deposition rate is modest to nearly negligible as shown on the sensitivity analysis based on stepwise increasing air exchange rate in section Pollutant deposition determination.

Appendix C: Residuals of the trained models

In Fig. 12, the residuals of the trained ET model is shown. From the figure, it is obvious that the mean value of the residuals is close to zero. However, the distribution is not normal. Due to this fact, the White test of heteroscedasticity was performed, resulting in rejecting heteroscedasticity.

On the other hand, GP and KNN residuals resulted in normal distribution according to the Shapiro test.

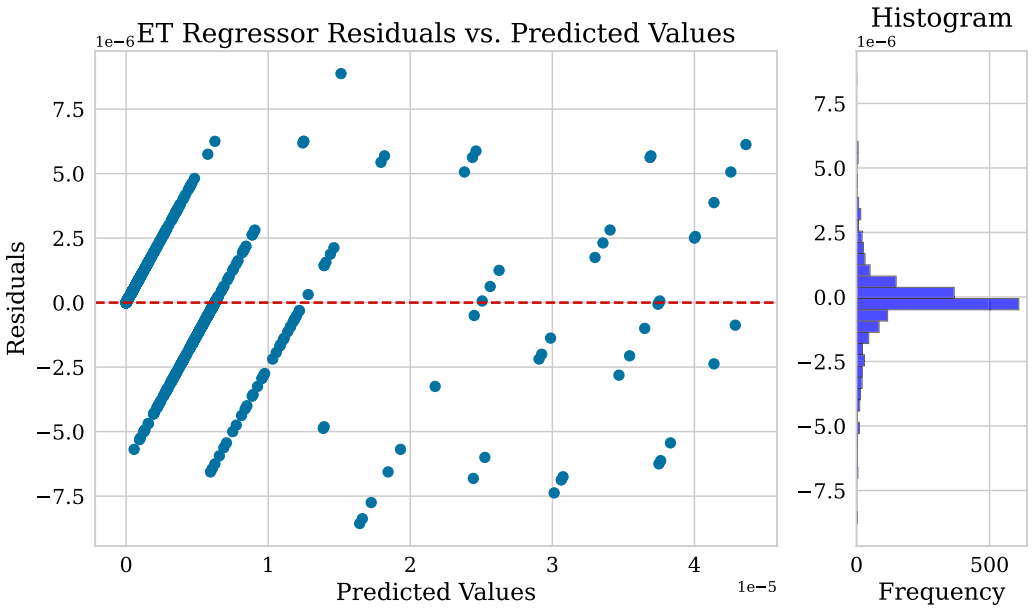

Fig. 12 Corrosion prediction error for ET regression

Abbreviations

ET: Extra trees
GP: Gaussian process
HVAC: Heating, ventilation, and air conditioning
IAQ: Indoor air quality
KNN: *k*-nearest neighbor
ML: Machine learning
PM: Particulate matter
VOC: Volatile organic compounds

Author Contributions

JF, MK[1], and CO were responsible for conceptualization, methodology, formal analysis, validation, writing, and editing of the paper. MK[1] and CO performed data mining and machine learning modeling; GS organized sensor installation, instrument calibration, and data collection at the site. TV and MK[2] supervised and reviewed the paper; EG and JE were responsible for project management and funding acquisition; All authors contributed to the final manuscript. All authors read and approved the final manuscript.

Funding

This research was carried out in the scope of the PROCRAFT project within the JPICH Conservation and Protection Call, supported by the following national funding organizations: Agence Nationale de la Recherche (ANR, France), Ministry of Universities and Research (MUR, Italy) and Ministry of Education, Youth and Sports (MEYS, Czech Republic).

Availability of data and materials

Datasets acquired and analyzed in this study are available in the Zenodo repository: https://zenodo.org/records/10640939. Developed models trained and used for prediction in this study are available in the GitHub repository: https://github.com/CVUT-FS-12110/Procraft_Corrosion_Model/tree/master.

Declarations

Competing interests

The authors declare that they have no competing interests.

Received: 28 October 2023 Accepted: 14 March 2024
Published online: 27 March 2024

References

1. Brimblecombe P, Grossi CM. Millennium-long damage to building materials in London. Sci Total Environ. 2009;407:1354–61.
2. Tidblad J. Atmospheric corrosion of heritage metallic artefacts: processes and prevention. UK: Woodhead Publishing Limited; 2013. p. 37–52.
3. Brimblecombe, P.: In: Lefevre, R.-A., Sabbioni, C. (eds.) Heritage climatology, pp. 57–64. Edipuglia, Bari, Italy (2010)
4. Tidblad J, Mikhailov AA, Kucera V. Model for the prediction of the time of wetness from average annual data on relative air humidity and air temperature. Prot Met. 2000;36:533–40.
5. Watkinson D. Conservation, corrosion science and evidence-based preservation strategies for metallic heritage artefacts. Cambridge, UK: Woodhead Publishing Limited; 2013. p. 9–36.
6. Kreislova K, Knotkova D, Geiplova H. Atmospheric corrosion of historical industrial structures. Cambridge, UK: Woodhead Publishing Limited; 2013. p. 311–43.
7. Castanié B, Bouvet C, Ginot M. Review of composite sandwich structure in aeronautic applications. JCOMC. 2020;1: 100004.
8. Brunet M, Cochard A, Deshayes C, Brouca-Cabarrecq C, Robbiola L, Olivier JM, Sciau P. Study of post-World War II French aeronautical aluminium alloy and coatings: historical and materials science approach. Stud Conserv. 2020;65:103–17.
9. Mutchler W. The weathering of aluminum alloy sheet materials used in aircraft. Washington, D.C: National Advisory Committee for Aeronautics; 1934. p. 1–38.
10. Gui F. Novel corrosion schemes for the aerospace industry. Amsterdam: Elsevier Science; 2009. p. 248–65.
11. Paz Martínez-Viademonte M, Abrahami ST, Hack T, Burchardt M, Terryn H. A review on anodizing of aerospace aluminum alloys for corrosion protection. Coatings. 2020;10:1106.
12. Berlanga-Labari C, Biezma-Moraleda MV, Rivero PJ. Corrosion of cast aluminum alloys: a review. Metals. 2020;10:1384.
13. Kuchariková L, Liptáková T, Tillová E, Kajánek D, Schmidová E. Role of chemical composition in corrosion of aluminum alloys. Metals. 2018;8:581.
14. Hallam D. Preventive conservation and maintenance of aluminium artefacts and collections. In: Proceedings from the the 2014 International Conference 'Aluminum: History, Technology, and Conservation, Smithsonian American Art Museum, Washington, D.C., pp. 199–208. 2014
15. Vargel C. Corrosion of aluminium. Oxford, UK: Elsevier Science; 2004. p. 81–291.
16. Carlos CAE, Velino C, Brunet M, Robbiola L, Bernardi E, Martini C, Chiavari C, Balbo A, Guilminot E. Galvanic corrosion over World War II aircraft wrecks. In: Proceedings of the EUROCORR 2022, Berlin, Germany. 2022.
17. Kramer P, Curtin T, Merrill M, Kim M, Friedersdorf F, Adey R. Atmospheric corrosion measurements to improve understanding of galvanic corrosion of aircraft. In: Proceedings of the CORROSION 2018, Phoenix, Arizona (2018). NACE-2018-10968, 2018.
18. Kosaba T, Muto I, Sugawara Y. Effect of anodizing on galvanic corrosion resistance of Al coupled to Fe or type 430 stainless steel in diluted synthetic seawater. Corros Sci. 2021;179: 109145.
19. Budinski KG, Budinski MK. Engineering materials: properties and selection. 9th ed. Upper Saddle River: Prentice Hall; 2010. p. 532–615.
20. Melchers RE. Modelling the long term atmospheric corrosion of aluminium alloys. Research Report 278.04.2010, The University of Newcastle, New South Wales, Australia. 2010.
21. Byrne SC, Miller AC. Effect of atmospheric pollutant gases on the formation of corrosive condensate on aluminum. Philadelphia: ASTM; 1982. p. 359–73.
22. Graedel J. Corrosion mechanisms for aluminum exposed to the atmosphere. J Electrochem Soc. 1989;136:204–12.
23. Diler E, Peltier F, Becker J, Thierry D. Real-time corrosion monitoring of aluminium alloys under chloride—contaminated atmospheric conditions. Corros Mater. 2021;72:1377–87.
24. Alebic-Juretic A. Airborne ammonia and ammonium within the Northern Adriatic area, Croatia. Environ Pollut. 2008;154:439–47.
25. Damborenea JD, Conde A. Comparison of accelerated and atmospheric exposure tests for corrosion of aluminium alloys. Br Corros J. 1995;30:292–6.
26. Sun S, Zheng Q, Li D, Wen J. Long-term atmospheric corrosion behaviour of aluminium alloys 2024 and 7075 in urban, coastal and industrial environments. Corros Sci. 2009;51:719–27.
27. Schindelholz E, Kelly RG, Cole IS, Ganther WD, Muster TH. Comparability and accuracy of time of wetness sensing methods relevant for atmospheric corrosion. Corros Sci. 2013;67:233–41.
28. Knotková-Čermáková D, Bartoň K. Corrosion aggressivity of atmospheres (derivation and classification). Philadelphia: ASTM; 1982. p. 225–49.
29. El-Mahdy GA, Kim KB. AC impedance study on the atmospheric corrosion of aluminum under periodic wet–dry conditions. Electrochim Acta. 2004;49:1937–48.
30. Pavlogeorgatos G. Environmental parameters in museums. Build Environ. 2003;38:1457–62.
31. Niklasson A, Johansson LG, Svensson JE. The influence of relative humidity and temperature on the acetic acid vapour-induced atmospheric corrosion of lead. Corros Sci. 2008;50:3031–7.
32. Gibson A, Johansson LG, Svensson JE. Acetic and formic acids emitted from wood samples and their effect on selected materials in museum environments. Corros Sci. 2010;52:172–8.
33. Prosek T, Taube M, Dubois F, Thierry D. Application of automated electrical resistance sensors for measurement of corrosion rate of copper, bronze and iron in model indoor atmospheres containing short-chain volatile carboxylic acids. Corros Sci. 2014;87:376–82.
34. Schindelholz E, Kelly RG. Wetting phenomena and time of wetness in atmospheric corrosion: a review. Corros Rev. 2012;30:135–70.

35. Macha EN, Dante JF, DeCarlo EC. Development of a methodology to predict atmospheric corrosion severity using corrosion sensor technologies. In: Proceedings of the CORROSION 2019, Nashville, Tennessee. 2019. NACE-2019-13389.
36. Turgoose S. Post-excavation changes in iron antiquities. Stud Conserv. 1982;27:97–101.
37. Grøntoft T, Raychaudhuri MR. Compilation of tables of surface deposition velocities for O_3, NO_2 and SO_2 to a range of indoor surfaces. Atmos Environ. 2004;38:533–44.
38. Lin JJ, Noll KE, Holsen TM. Dry deposition velocities as a function of particle size in the ambient atmosphere. Aerosol Sci Technol. 1994;20:239–52.
39. Dean SW, Reiser DB. Comparison of atmospheric corrosion rates of wires and flat panels. In: Proceedings of the CORROSION 2000, Orlando, Florida. NACE-00455, 2000.
40. Grzywacz CM. Monitoring for gaseous pollutants in museum environments—(tools for conservation). Los Angeles, CA: Getty Publications; 2006. p. 21–72.
41. Tétreault J. Airborne pollutants in museums, galleries and archives: risk assessment. Ottawa, Canada: Control Strategies and Preservation Management. Canadian Conservation Institute. 2004. p. 7–138.
42. Ahuir-Torres JI, Simandjuntak S, Bausch N, Farrar A, Webb S, Nash A, et al. Corrosion threshold data of metallic materials in various operating environment of offshore wind turbine parts (tower, foundation, and nacelle/gearbox). Data Br. 2019;25: 104207.
43. Mašková L, Smolík J, Ondráček J, Ondráčková L, Trávníčková T, Havlica J. Air quality in archives housed in historic buildings: assessment of concentration of indoor particles of outdoor origin. Build Environ. 2020;180: 107024.
44. Strlič M, Grau-Bové J. Fine particulate matter in indoor cultural heritage: a literature review. Herit Sci. 2013;1:8.
45. Saraiva NB, Pereira LD, Gaspar AR, Costa JJ. Measurement of particulate matter in a heritage building using optical counters: long-term and spatial analyses. Sci Total Environ. 2023;862: 160747.
46. Bertolin C, Strojecki M, Kozłowski R. Particle penetration, emission and deposition in the Diocesan Museum in Udine, Italy to Assess Soiling of Giambattista Tiepolo's Wall Paintings. Stud Conserv. 2018;63:326–8.
47. Chatoutsidou SE, Mašková L, Ondráčková L, Ondráček J, Lazaridis M, Smolík J. Modeling of the aerosol infiltration characteristics in a cultural heritage building: the Baroque Library Hall in Prague. Build Environ. 2015;89:253–63.
48. Serfozo N, Chatoutsidou SE, Lazaridis M. The effect of particle resuspension during walking activity to PM_{10} mass and number concentrations in an indoor microenvironment. Build Environ. 2014;82:180–9.
49. Rosati JA, Thornburg J, Rodes C. Resuspension of particulate matter from carpet due to human activity. Aerosol Sci Technol. 2008;42:472–82.
50. Kontozova-Deutsch V, Cardell C, Urosevic M, Ruiz-Agudo E, Deutsch F, Van Grieken R. Characterization of indoor and outdoor atmospheric pollutants impacting architectural monuments: the case of San Jerónimo Monastery (Granada, Spain). Environ Earth Sci. 2011;63:1433–45.
51. Ryhl-Svendsen M, Clausen G. The effect of ventilation, filtration and passive sorption on indoor air quality in museum storage rooms. Stud Conserv. 2009;54:35–48.
52. Yoon YH, Brimblecombe P. The distribution of soiling by coarse particulate matter in the museum environment. Indoor Air. 2001;11:232–40.
53. Ryhl-Svendsen M. Corrosivity measurements of indoor museum environments using lead coupons as dosimeters. J Cult Herit. 2008;9:285–93.
54. Hren I, Kusmierczak S, Kurajdov K. Microstructure analysis of corrosion resistance of cast AlCu4Mg1 alloy, vol. 9. Hoboken, New Jersey: Wiley; 2021. p. 31–5.
55. Benounis M, Jaffrezic-Renault N. Elaboration of an optical fibre corrosion sensor for aircraft applications. Sens Actuators B Chem. 2004;100:1–8.
56. Prosek T, Kouril M, Dubus M, Taube M, Hubert V, Scheffel B, Degres Y, Jouannic M, Thierry D. Real-time monitoring of indoor air corrosivity in cultural heritage institutions with metallic electrical resistance sensors. Stud Conserv. 2013;58:117–28.
57. Dubus M, Prosek T. Standardized assessment of cultural heritage environments by electrical resistance measurements. e-Preserv Sci. 2012;9:60–4.
58. Kouril M, Prosek T, Scheffel B, Degres Y. Corrosion monitoring in archives by the electrical resistance technique. J Cult Herit. 2014;15:99–103.
59. Diler E, Lédan F, LeBozec N, Thierry D. Real-time monitoring of the degradation of metallic and organic coatings using electrical resistance sensors. Corros Mater. 2017;68:1365–76.
60. Matthiesen H. Oxygen monitoring in the corrosion and preservation of metallic heritage artefacts. In: Dillmann P, Watkinson D, Angelini E, Adriaens A, editors. Corrosion and conservation of cultural heritage metallic artefacts. Cambridge, UK: Woodhead Publishing Limited; 2013. p. 368–91.
61. Matthiesen H, Wonsyld K. In situ measurement of oxygen consumption to estimate corrosion rates. Corros Eng Sci Technol. 2010;45:350–6.
62. Roberge PR, Klassen RD, Haberecht PW. Atmospheric corrosivity modeling—a review. Mater Des. 2002;23:321–30.
63. Macha EN, DeCarlo EC, Dante JF. Developing a likelihood-based modeling approach to predict atmospheric corrosion rates using corrosion sensor technologies. In: Proceedings of the CORROSION 2021 (2021). NACE-2021-16806.
64. Feliu S, Morcillo M, Feliu S Jr. The prediction of atmospheric corrosion from meteorological and pollution parameters-I. Annu Corros Sci. 1993;34:403–14.
65. Dean SW, Reiser DB. Analysis of long-term atmospheric corrosion results from ISO CORRAG program. In: Townsend H, editor. Outdoor Atmospheric Corrosion, ASTM STP 1421. West Conshohocken, PA: ASTM International; 2002. p. 3–18.
66. Mikhailov AA, Tidblad J, Kucera V. The classification system of ISO 9223 standard and the dose-response functions assessing the corrosivity of outdoor atmospheres. Prot Met. 2004;40:541–50.
67. Titakis C, Vassiliou P. Evaluation of 4-year atmospheric corrosion of carbon steel, aluminum, copper and zinc in a coastal military airport in Greece. Corros Mater Degrad. 2020;1:159–86.
68. Kuss M. Gaussian process models for robust regression, classification, and reinforcement learning. PhD thesis, Technische Universität Darmstadt, Darmstadt. 2006.
69. Chiavari C, Bernardi E, Balbo A, Monticelli C, Raffo S, Bignozzi MC, Martini C. Atmospheric corrosion of fire-gilded bronze: corrosion and corrosion protection during accelerated ageing tests. Corros Sci. 2015;100:435–47.
70. Sereda PJ, Croll SG, Slade HF. Effect of atmospheric pollutant gases on the formation of corrosive condensate on aluminum. In: Dean SW, Rhea EC, editors. Atmospheric Corrosion of Metals, ASTM STP 767. Philadelphia, PA: ASTM; 1982. p. 267–85.
71. Oswald C, Kuchař M, Fišer J, Khol M, Oswaldová I, Simeunović G, Vyhlídal T, Robbiola L, Brunet M, Monticelli C, Balbo A, Chiavari C, Martini C, Bernardi E, Guilminot E, Echinard J. Pollution and moisture infiltration effect assessment based on data-driven analysis for aircraft heritage protection. In: E3S Web of Conferences 356—16th ROOMVENT Conference (ROOMVENT 2022), Xi'an, China, p. 02052. 2022
72. Cai Y, Xu Y, Zhao Y, Ma X. Atmospheric corrosion prediction: a review. Corros Rev. 2020;38:299–321.
73. Abdul-Wahab SA. Statistical prediction of atmospheric corrosion from atmospheric-pollution parameters. Pract Period Hazard Toxic Radioact Waste Manage. 2003;7:190–200.
74. Engelhardt G, Macdonald DD. Unification of the deterministic and statistical approaches for predicting localized corrosion damage. I. theoretical foundation. Corros Sci. 2004;46:2755–80.
75. Melchers RE. Statistical characterization of pitting corrosion- part 2: probabilistic modeling for maximum pit depth. Corrosion. 2005;61:766–77.
76. Valor A, Caleyo F, Alfonso L, Rivas D, Hallen JM. Stochastic modeling of pitting corrosion: a new model for initiation and growth of multiple corrosion pits. Corros Sci. 2007;49:559–79.
77. Li X, Zhao Y, Qi W, Wang J, Xie J, Wang H, Chang L, Liu B, Zeng G, Gao Q, Sun H. Modeling of pitting corrosion damage based on electrochemical and statistical methods. J Electrochem Soc. 2019;166:539–49.
78. Jarrah A, Bigerelle M, Guillemot G, Najjar D, Iost A, Nianga JM. A generic statistical methodology to predict the maximum pit depth of a localized corrosion process. Corros Sci. 2011;53:2453–67.
79. Murer N, Buchheit RG. Stochastic modeling of pitting corrosion in aluminum alloys. Corros Sci. 2013;69:139–48.

80. Pidaparti RM, Palakal MJ, Fang L. Cellular automation approach to model aircraft corrosion pit damage growth. AIAA J. 2004;42:2562–9.
81. Long ER, Bone A, Breitung EM, Thickett D. Automated corrosion detection in Oddy test coupons using convolutional neural networks. Herit Sci. 2022;10:150.
82. Cavanaugh MK, Buchheit RG, Birbilis N. Modeling the environmental dependence of pit growth using neural network approaches. Corros Sci. 2010;52:3070–7.
83. Jimenez-Come MJ, Luz Martín M, Matres V. A support vector machine-based ensemble algorithm for pitting corrosion modeling of EN 1.4404 stainless steel in sodium chloride solutions. Mater Corros. 2019;70:19–27.
84. Coelho LB, Zhang D, Van Ingelgem Y, Steckelmacher D, Nowé A, Terryn H. Reviewing machine learning of corrosion prediction in a data-oriented perspective. NPJ Mater Degrad. 2022;6:8.
85. Diao Y, Yan L, Gao K. Improvement of the machine learning-based corrosion rate prediction model through the optimization of input features. Mater Des. 2021;198: 109326.
86. Boesgaard C, Hansen BV, Kejser UB, Mollerup SH, Ryhl-Svendsen M, Torp-Smith N. Prediction of the indoor climate in cultural heritage buildings through machine learning: first results from two field tests. Herit Sci. 2022;10:176.
87. Kuchař M, Fišer J, Oswald C, Khol M, Oswaldová I, Simeunović G, Vyhlídal T, Robbiola L, Brunet M, Balbo A, Chiavari C, Martini C, Bernardi E, Guilminot E, Echinard J. Hangar environment monitoring for corrosion risk assessment and aeronautical heritage protection. In: Proceedings of the 2023 24th Int. Conf. Process Control (PC 2023), High Tatras, Slovakia. 2023; p. 256–60.
88. Degrigny C. Stabilisation de moteurs d'avions immergés. Stud Conserv. 1995;40:10–8.
89. Degrigny C. La conservation-restauration de l'aluminium aéronautique: regard rétrospectif. Cahiers d'histoire de l'aluminium. 2021;66:30–9.
90. Rocca E, Mirambet F, Tilatti C. Long term corrosion of aluminium materials of heritage: analysis and diagnosis of aeronautic collection. Corros Eng Sci Technol. 2010;45:345–9.
91. Brunet M, Robbiola L, Deshayes C, Bernardi E, Martini C, Chiavari C, Balbo A, Monticelli C, Fišer J, Vyhlídal T, Echinard J, Guilminot E. First step in the PROCRAFT Project on WWII aircraft heritage: Investigation and conservation of the aluminium alloys. In: Proceedings of the METAL 2022, Helsinki, Finland. 2022.
92. Montané C, Velino C, André E, Aufray M, Gayet F, Robbiola L, Brouca-Cabarrecq C, Sciau P, Brunet M. Historical primers and paints used for aeronautical protection and colouring during WWII: a multi-techniques approach on archaeological parts. J Cult Herit. 2023;62:54–64.
93. Military History Institute Prague: The Aviation Museum Kbely. Accessed: 10 Feb 2023. 2023. https://www.vhu.cz/en/english-summary.
94. Khol M, Rajlich J, Sýkora J. Catalogue of the Aviation Museum. The Ministry of Defence of the Czech Republic—the Military History Institute Prague, Prague, Czech Republic. 2017. pp. 9–134.
95. Becker J, Diler E. Atmospheric corrosion loggers. Accessed: 10 Feb 2023 (2023). https://www.institut-corrosion.fr/activities/aircorr-loggers-aircorr/?lang=en.
96. Eltek Ltd. Touring Transmitters with built-in temperature/RH and temperature sensors. Accessed 10 Feb 2023. 2023. https://www.eltekdataloggers.co.uk/.
97. Kilinççeker G, Taze N, Galip H, Yazici B. The effect of sulfur dioxide on iron, copper and brass. Anti-Corros Methods Mater. 2011;58:4–12.
98. Czech Hydrometeorological Institute: Information about air quality in the Czech Republic: Measuring programme table ARIEA. Accessed: 23 Jan 2024. 2024. https://www.chmi.cz/files/portal/docs/uoco/web_generator/locality/pollution_locality/mp_ARIEA_GB.html.
99. Czech Hydrometeorological Institute: Information about air quality in the Czech Republic: Measuring programme table AHOLA. Accessed: 23 Jan 2024. 2024. https://www.chmi.cz/files/portal/docs/uoco/web_generator/locality/pollution_locality/mp_AHOLA_GB.html.
100. ISO 9223: Corrosion of metals and alloys—corrosivity of atmospheres—classification, determination and estimation, 2nd edn, pp. 1–15. ISO, Geneva, Switzerland. 2012.
101. Dongarrà G, Manno E, Varrica D, Lombardo M, Vultaggio M. Study on ambient concentrations of PM10, PM10-25, PM25 and gaseous pollutants. Trace elements and chemical speciation of atmospheric particulates. Atmos Environ. 2010;44:5244–57.
102. Utah Department of Environmental Quality: Particulate Chloride in the Urban Environment. Accessed: 15 Jan 2024. 2024. https://deq.utah.gov/air-quality/particulate-chloride-in-the-urban-environment.
103. Ryhl-Svendsen M. Indoor air pollution in museums: prediction models and control strategies. Stud Conserv. 2006;51:27–41.
104. ASHRAE: Chapter 23: Museums, Galleries, Archives, and Libraries, pp. 1–22. ASHRAE, Atlanta, GA. 2015.
105. Ali M. PyCaret: an open source, low-code machine learning library in Python. Accessed: 10 July 2023 (2020). https://www.pycaret.org.

Publisher's Note